recycling

MDPI

Article

Waste-on-Waste Roasting of Copper Slag with Flotation Tailings for Selective Recovery of Cu, Ni, and Co

Bobur Gayratov [1,*], Bekhzod Gayratov [1], Labone L. Godirilwe [2], Gwiranai Danha [3] and Atsushi Shibayama [2,*]

[1] Graduate School of International Resource Sciences, Akita University, 1-1, Tegata-Gakuenmachi, Akita 010-8502, Japan; bmgayratov@gmail.com
[2] Faculty of International Resource Sciences, Akita University, 1-1, Tegata-Gakuenmachi, Akita 010-8502, Japan; llgodirilwe@gipc.akita-u.ac.jp
[3] Department of Chemical, Materials & Metallurgical Engineering, Botswana International University of Science & Technology, Private Bag 16, Palapye 10071, Botswana; danhag@biust.ac.bw
* Correspondence: bobur.gayratov@gmail.com (B.G.); sibayama@gipc.akita-u.ac.jp (A.S.)

Abstract

Copper smelter slag represents a significant secondary resource of critical metals, while flotation tailings serve as an abundant sulfur-bearing waste stream. This study investigated a waste-on-waste sulfation roasting approach for the selective recovery of Cu, Ni, and Co from fayalite copper smelter slag using flotation tailings as an in situ sulfur source and sodium metabisulfite (SMBS, $Na_2S_2O_5$) as a sulfation promoter. The effects of roasting temperature, roasting time, slag-to-tailings ratio, SMBS dosage, and water-leaching conditions were systematically evaluated. Under the optimum conditions of a slag-to-tailings ratio of 1:1, roasting at 600 °C for 4 h with 30 wt% SMBS addition, followed by water leaching at 25 °C for 2 h, extraction efficiencies of 85.5% Cu, 81.6% Ni, and 87.1% Co were achieved, while Fe dissolution remained below 5%, demonstrating high selectivity. Phase and microstructural analyses by XRD, FTIR, SEM, and TG–DTA revealed that pyrite oxidation generated sulfur oxides required for metal sulfation, whereas SMBS promoted sulfur release and sulfate stabilization, enhancing sulfation efficiency. Thermodynamic analysis further confirmed the feasibility of sulfide oxidation and sulfate formation within the investigated temperature range. The results demonstrate that the synergistic use of tailings and SMBS enables efficient low-temperature sulfation roasting of fayalite slag and provides a promising route for the selective recovery of valuable metals from metallurgical waste materials.

Keywords: fayalite slag; flotation tailings; sulfation roasting; leaching; sodium metabisulfite; waste-on-waste processing; secondary resources

Check for updates

Academic Editor: Jack Groppo

Received: 30 May 2026
Revised: 9 July 2026
Accepted: 11 July 2026
Published: 14 July 2026

Copyright: © 2026 by the authors. Licensee MDPI, Basel, Switzerland. This article is an open access article distributed under the terms and conditions of the Creative Commons Attribution (CC BY) license.

1. Introduction

The global demand for metallic mineral resources has been rising steadily due to worldwide industrialization and digitalization. This trend has been further accelerated by the recently proclaimed green energy transition aimed at replacing fossil fuels with wind, solar, hydrogen, and geothermal energy [1]. Accordingly, critical metals have become indispensable, not only for enabling low-carbon technologies but also for driving innovation in resource-efficient extraction methods [2]. However, growing concerns regarding supply constraints and geological scarcity have increased attention toward circular economy strategies and the utilization of secondary resources [3]. Because such materials may contain economically significant concentrations of critical metals, their processing has

become increasingly important in response to the rising demand for raw materials required for low-carbon and energy-transition technologies [4,5].

The transition from fossil-based energy systems to renewable technologies has significantly increased global dependence on critical metals required for low-carbon applications, including Cu, Ni, Co, Zn, and platinum-group metals [6]. Among the metals most at risk of supply shortfalls, cobalt stands out given its geographic concentration and growing end-use demand. Against this backdrop, anthropogenic waste streams, particularly copper smelter slag and flotation tailings, have attracted growing interest as secondary metal resources because they can reduce dependence on primary ores while simultaneously mitigating waste-related environmental issues [7].

Copper smelter slag is a major metallurgical byproduct generated during pyrometallurgical copper production and commonly contains significant concentrations of Fe and valuable metals [8,9]. The accumulation of large quantities of copper slag occupies a substantial land area. In addition, wind erosion and rainfall can mobilize heavy metals and sulfide-bearing species into soils and groundwater, causing environmental pollution [10,11]. Similarly, flotation tailings, which often contain pyrite, residual metal sulfides, and reagents, may create serious ecological problems over time if tailings facilities are not properly stabilized [12]. As metal reserves and head grades continue to decline, such secondary resources are increasingly regarded as viable raw materials [13].

Various pyrometallurgical and hydrometallurgical methods have been investigated for the treatment of copper smelter slag, including flotation, carbothermic reduction, direct acid leaching, pressure leaching, and combined roasting–leaching processes. The results of some relevant studies are summarized in Table 1.

Table 1. Summary of relevant studies on Cu, Ni, Co, Fe extraction from copper slag.

Slag Type	Treatment Method	Roasting Reagents	Recovery Efficiency, %				Reference
			Cu	Ni	Co	Fe	
Converter slag	Roasting, water leaching	$(NH_4)_2SO_4$ H_2SO_4	85 95	81 90	85 99	- -	[14]
Smelter and converter slag	Preroasting, roasting, water leaching	FeS_2	95	36	98	2.7	[15]
Converter slag	Roasting, water leaching	$Fe_2(SO_4)_3$	93	13	38	-	[16]
Smelter slag	Leaching with sulfuric acid, sodium chlorate oxidant	-	89	-	98	0.02	[17]
Converter slag	High pressure oxidative leaching (HPOL) with pyrrhotite tailings	-		95–97		-	[18]
Smelter slag	Bioleaching	-	44	4.5	13	-	[19]
Smelter slag	Roasting, decomposition roasting, water leaching	H_2SO_4	74.2	71.1	69.6	4.9	[20]
Smelter slag	Alkali disaggregation, acid leaching	-	99.9	-	-	41.5	[21]
Smelter slag	Roasting, water leaching	SO_2-O_2-Ar, Na_2SO_4	81.6	95.8	91.8	5	[22]
Smelter slag	Sulfuric acid leaching	-	97	98	86	88	[11]
Smelter slag	High pressure oxidative leaching (HPOL)	-	89.4	99.9	99.9	7.2	[23]
Copper slag	Roasting, sulfuric acid leaching	Charcoal, $Na_2B_4O_7$	77.3	-	83.3	86.5	[24]

Flotation is the most widely applied beneficiation method for the recovery of valuable metals from smelter slags [25,26]. The process is effective for recovering liberated sulfide phases. However, metals such as Co are often poorly recovered because they predominantly occur in oxide forms or remain encapsulated within the fayalite matrix. As a result, extensive fine grinding is required to achieve sufficient liberation [27,28]. Carbothermic reduction can recover valuable metals through alloy formation, but the process typically requires temperatures above 1400 °C and involves high energy consumption [29,30]. Direct leaching of amorphous fayalite slags is also challenging because the glassy silicate structure is relatively resistant to dissolution under conventional leaching conditions [31]. High-pressure leaching (HPL) has been investigated as a method to enhance metal recovery from amorphous slags [32]. However, the process remains economically unfavorable due to significant equipment and operating costs, as well as the production of large quantities of waste residues [33,34]. Therefore, efficient and potentially sustainable approaches for the treatment of amorphous fayalite slags remain necessary to improve resource recovery and mitigate environmental concerns.

Pyrite-rich flotation tailings represent a promising alternative sulfur source for sulfation roasting because pyrite oxidation generates sulfur-bearing gases (SO_2 and SO_3) required for the formation of water-soluble metal sulfates. Previous studies have successfully utilized pyrite as a sulfur donor during the sulfidation roasting of zinc leaching residues, zinc oxide minerals, and copper smelter slags. The gradual decomposition of pyrite provided a continuous sulfur supply, thereby promoting phase transformation and improving metal recovery [15,35,36]. During roasting, pyrite undergoes progressive oxidation and decomposition reactions, producing SO_2 and SO_3 while simultaneously transforming iron sulfides into relatively stable iron oxide phases. Consequently, the utilization of pyrite-bearing tailings as an in situ sulfur source offers the opportunity to simultaneously valorize two metallurgical waste streams within a single integrated process while reducing the consumption of external sulfur-containing reagents. Nevertheless, the sulfation behavior of fayalite copper slag during co-roasting with pyrite-rich tailings, particularly under low-temperature conditions and in the presence of sulfation promoters, remains insufficiently understood.

In the present study, a novel waste-on-waste approach is proposed for the recovery of cobalt, nickel, and copper from amorphous fayalite slag through co-treatment with pyrite-rich flotation tailings. Unlike previous studies that primarily employed commercial sulfur-bearing reagents or individual sulfur donors for sulfation roasting, the present study utilizes flotation tailings as an in situ sulfur source. Sodium metabisulfite (SMBS, $Na_2S_2O_5$) is added as an additional sulfur-oxide promoter during relatively low-temperature roasting, followed by water leaching. The proposed integrated slag-tailings co-treatment strategy simultaneously valorizes two metallurgical waste streams and achieves selective extraction of Cu, Ni, and Co with minimal iron dissolution. This approach may provide an alternative route for the utilization of abandoned tailings and smelter slags and could potentially contribute to future mine remediation and metallurgical waste-management strategies.

2. Results and Discussion

2.1. Thermodynamic Analysis

Based on the experimental results, the sulfation roasting of fayalite slag can be divided into three sequential stages.

In the first stage, oxidation of metal sulfides occurs. In the presence of oxygen, copper and nickel present as sulfide matte inclusions within the slag matrix, together with pyrite, are oxidized to their corresponding oxides, accompanied by the release of sulfur dioxide according to Reaction (R1), where Me represents Cu, Ni, or Fe. Simultaneously, sulfur

dioxide is further oxidized to sulfur trioxide under oxidizing conditions, as described by Reaction (R2):

$$MeS + 3/2O_2 = MeO + SO_2 \quad (R1)$$

$$2SO_2 + O_2 = 2SO_3 \quad (R2)$$

Pyrite oxidation during sulfation roasting is a complex multistep process that likely proceeds through transient pyrrhotite and iron oxide intermediates prior to the formation of stable hematite under oxidizing conditions [37]. Initially, pyrite undergoes partial thermal decomposition to form pyrrhotite-like phases according to Reaction (R3). Subsequently, the intermediate iron sulfide phases are oxidized to iron oxides with the release of sulfur dioxide (Reaction (R4)), while further oxidation of FeO leads to the formation of hematite (Reaction (R5)):

$$FeS_2 = Fe_{1-x}S + S \quad (R3)$$

$$Fe_{1-x}S + O_2 = FeO + SO_2 \quad (R4)$$

$$4FeO + O_2 = 2Fe_2O_3 \quad (R5)$$

The sulfur dioxide released during these transformations can be further oxidized to SO_3, thereby contributing to the sulfation of Cu-, Ni-, and Co-bearing phases. Under the investigated roasting conditions, hematite was identified as the dominant iron-containing phase in the calcines, indicating that the transient intermediate phases were progressively converted into stable iron oxides during roasting. In the second stage, the metal oxides formed during sulfide oxidation undergo sulfation reactions. The metal oxides react with sulfur trioxide to form metal sulfates (Reaction (R6)). In addition, direct sulfation of metal oxides can proceed via the combined action of sulfur dioxide and oxygen, resulting in the formation of metal sulfates through Reaction (R7):

$$MeO + SO_3 = MeSO_4 \quad (R6)$$

$$2MeO + 2SO_2 + O_2 = 2MeSO_4 \quad (R7)$$

These reactions are promoted by the progressive decomposition of the fayalite matrix into ferric oxide and silica, which liberates metal-bearing phases and enhances their accessibility to sulfur oxides. The standard Gibbs free energy changes and corresponding equilibrium constants (K) for the relevant reactions were calculated using HSC Chemistry 10 [38]. The thermodynamic results are summarized in Table 2, while the temperature dependence of the Gibbs free energy changes is presented in Figure 1, confirming the thermodynamic feasibility of sulfide oxidation and subsequent sulfation within the investigated temperature range.

In the third stage, the extraction efficiencies of valuable metals increased significantly with the addition of SMBS during roasting. SMBS acts as an effective sulfation promoter by simultaneously enhancing the sulfur oxide potential and improving solid-state mass transfer during roasting.

At relatively low temperatures (150–300 °C), SMBS undergoes rapid thermal decomposition, releasing reactive sulfur oxides according to Reaction (R8):

$$Na_2S_2O_5 = Na_2SO_3 + SO_2 \quad (R8)$$

Table 2. Reaction equations occurring during sulfation roasting.

No	Reaction Equations	$\Delta G^0 = \Delta H - T\Delta S$ (kJ/mol)		ΔG^0	LogK
		ΔH (kJ/mol)	ΔS (kJ/mol·^{0}C)	600 °C	600 °C
1	$CuS + 1.5O_2(g) = CuO + SO_2(g)$	−401.139	−0.088	−323.668	19.365
2	$NiS + 1.5O_2(g) = NiO + SO_2(g)$	−448.870	−0.085	−374.977	22.434
3	$FeS_2 + 2.5O_2(g) = FeO + 2SO_2(g)$	−687.748	−0.012	−677.400	40.528
4	$4FeS_2(g) + 11O_2(g) = 2Fe_2O_3 + 8SO_2(g)$	−3326.314	−297.510	−3066.543	183,466
5	$2SO_2(g) + O_2(g) = 2SO_3(g)$	−197.011	−0.188	−33.250	1.990
6	$CuO + SO_3(g) = CuSO_4$	−211.011	−0.174	−58.811	3.520
7	$NiO + SO_3(g) = NiSO_4$	−231.161	−0.183	−71.201	4.260
8	$CoO + SO_3(g) = CoSO_4$	−245.042	−0.177	−90.392	5.408
9	$FeO + SO_3(g) = FeSO_4$	−260.195	−0.183	−100.524	6.014
10	$2CuO + 2SO_2(g) + O_2(g) = 2CuSO_4$	−619.033	−0.536	−150.869	9.026
11	$2NiO + 2SO_2(g) + O_2(g) = 2NiSO_4$	−659.334	−0.554	−175.650	10.509
12	$2CoO + 2SO_2(g) + O_2(g) = 2CoSO_4$	−687.096	−0.542	−214.030	12.810
13	$2FeO + 2SO_2(g) + O_2(g) = 2FeSO_4$	−717.401	−0.553	−234.295	14.017

The generated sodium sulfite is readily oxidized in the presence of oxygen to form sodium sulfate (Reaction (R9)), while SMBS can also undergo direct oxidative conversion to sodium sulfate with simultaneous SO_2 release (Reaction (R10)):

$$Na_2SO_3 + 0.5O_2 = Na_2SO_4 \quad (R9)$$

$$Na_2S_2O_5 + 0.5O_2 \rightarrow Na_2SO_4 + SO_2 \quad (R10)$$

The SO_2 generated from these reactions is further oxidized to SO_3 at elevated temperatures, providing a highly reactive sulfating atmosphere. Concurrently, sodium sulfate formed in situ acts as a sulfate carrier and reaction medium, participating in sulfate-transfer reactions with metal sulfides and oxides (Reactions (R11) and (R12)):

$$MeS + Na_2SO_4 = MeSO_4 + Na_2S \quad (R11)$$

$$MeO + Na_2SO_4 + 1/2O_2 + SO_2 = MeSO_4 \cdot Na_2SO_4 \quad (R12)$$

The formation of alkali–metal sulfate phases derived from SMBS enhances sulfation roasting by increasing particle porosity, improving gas–solid interactions, and facilitating the diffusion of sulfur oxides toward reactive metal-bearing phases [39]. In addition, the formation of eutectic double-sulfate compounds such as $Na_2Me(SO_4)_2$, according to Reaction (R13), enhances the thermal stability of $CuSO_4$, $NiSO_4$, and $CoSO_4$, thereby suppressing their premature thermal decomposition and promoting higher sulfate retention during roasting [40,41]:

$$Na_2SO_4 + MeSO_4 = MeSO_4 \cdot Na_2SO_4 \quad (R13)$$

The flowsheet and overall sulfation roasting mechanism of the slag, schematically illustrated in Figure 2, can be described as follows. Copper and nickel are initially present in the slag as sulfide phases, while cobalt predominantly exists in oxide form. During roasting, the fayalite matrix decomposes into ferric oxide and silica, liberating metal-bearing phases and facilitating subsequent sulfation reactions. The addition of SMBS significantly enhances sulfation kinetics by generating additional SO_3 and forming molten eutectic sulfate phases, which collectively promote the conversion of Cu, Ni, and Co into stable, water-soluble

sulfates. These sulfates are readily dissolved during subsequent water leaching under optimal conditions, resulting in substantially increased metal extraction efficiencies.

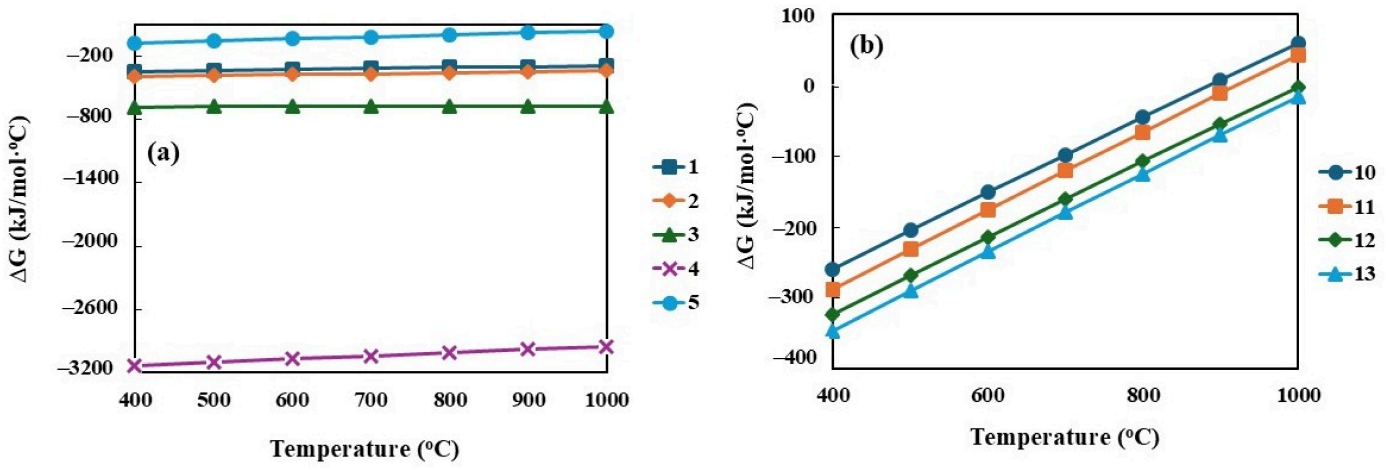


Figure 1. Thermodynamic calculation of (**a**) the oxidation and (**b**) the sulfation processes. Calculated using HSC Chemistry 10 software.

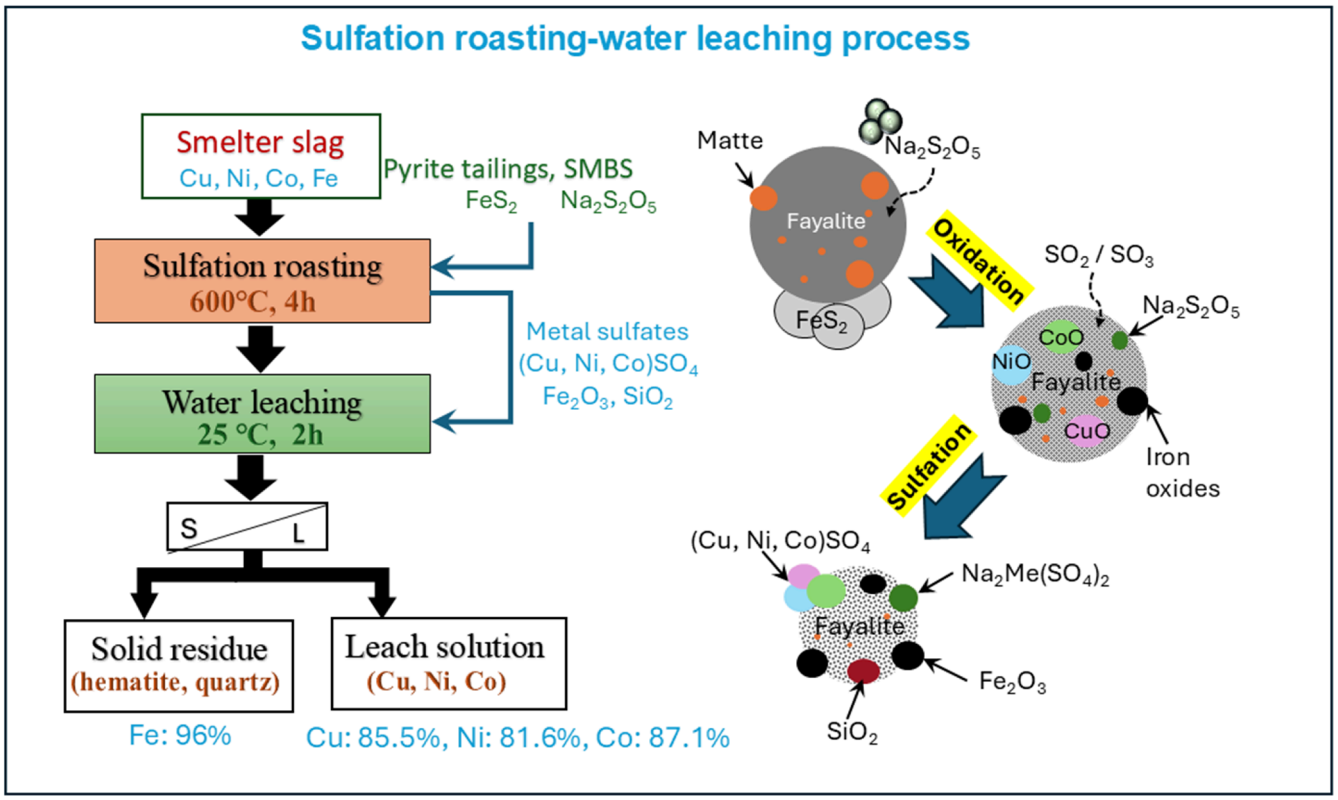


Figure 2. Flowsheet and schematic diagram of roasting–leaching process.

2.2. Roasting

2.2.1. Effect of Roasting Temperature

To further evaluate the necessity of sulfation roasting prior to leaching, direct leaching experiments were conducted on the raw fayalite slag without any thermal pre-treatment. The results showed negligible dissolution of Cu, Ni, and Co under the investigated leaching conditions, with extraction efficiencies remaining close to 0%. This behavior confirms the refractory nature of the water-quenched fayalite slag and indicates that the valuable metals are strongly immobilized within sulfide matte inclusions and silicate-associated phases.

The effect of roasting temperature on the extraction efficiencies of copper, nickel, cobalt, and iron was systematically evaluated in the range of 450–700 °C. The experiments were performed using a fixed slag-to-tailings mass ratio of 1:1, a roasting duration of 4 h, and subsequent water leaching for 1 h at 25 °C under a pulp density of 10% and shaking speed of 180 rpm. The corresponding mass variations of the calcined products are shown in Figure 3, revealing temperature-dependent changes associated with gas evolution, oxidation, and sulfation reactions. The weight increase ratio, α, was determined using Equation (1):

$$\alpha(\%) = \frac{\Delta m}{m_{raw}} \times 100 \quad (1)$$

where Δm is the mass change during roasting and m_{raw} is the initial sample mass.

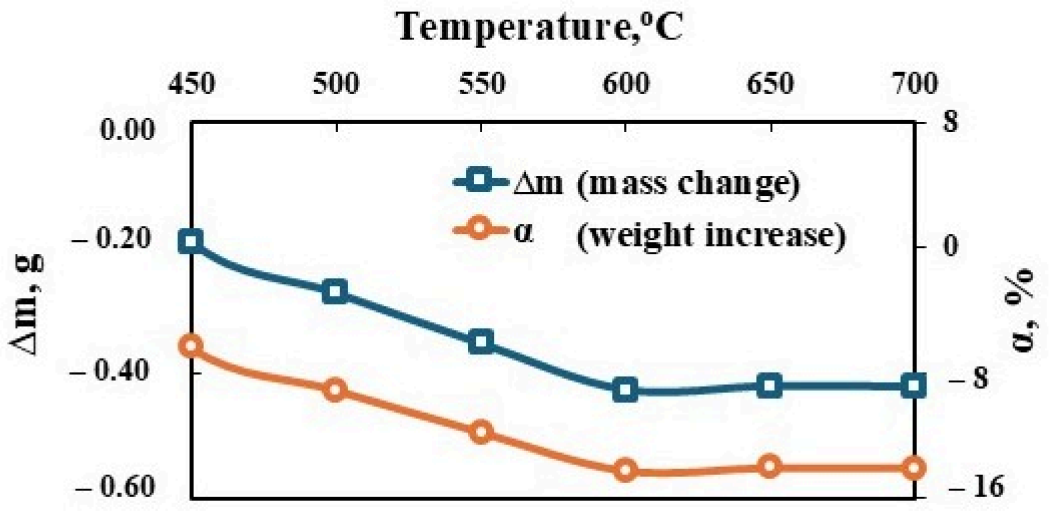


Figure 3. Weight change of samples after roasting.

All samples experienced mass loss after sulfation roasting, with the highest loss observed at 600 °C. The XRD patterns of roasted products at different temperatures are presented in Figure 4. Metal sulfate phases became detectable at 550–650 °C, while iron sulfate species appeared at 450 and 500 °C, indicating the early formation of sulfates through pyrite oxidation. However, partial thermal decomposition of these sulfates commenced near 450 °C, and at higher temperatures, substantial mass loss resulted from progressive oxidation and volatilization of sulfur-bearing species.

As the temperature increased, new crystalline phases such as hematite and quartz were formed, reflecting the breakdown of the primary fayalite structure. Nevertheless, residual fayalite peaks remained even at elevated temperatures, suggesting incomplete phase transformation and potential encapsulation of valuable metals within the silicate matrix. Sulfates containing target metals were therefore difficult to detect at these higher temperatures. At 700 °C, hematite was identified as the dominant phase.

After roasting, the calcined materials were leached with distilled water under controlled conditions (1 h, 25 °C, 10% pulp density, 180 rpm). The extraction yields of the target metals are presented in Figure 5a. The temperature-dependent leaching behavior aligned well with previous studies [41,42] and corresponded closely to the mass-loss trends observed in Figure 3. Among the valuable metals, nickel demonstrated the highest extraction efficiency, followed by copper and cobalt. Maximum extractions were achieved at 600 °C, reaching 74.1% for Ni, 68.3% for Cu, and 54.3% for Co.

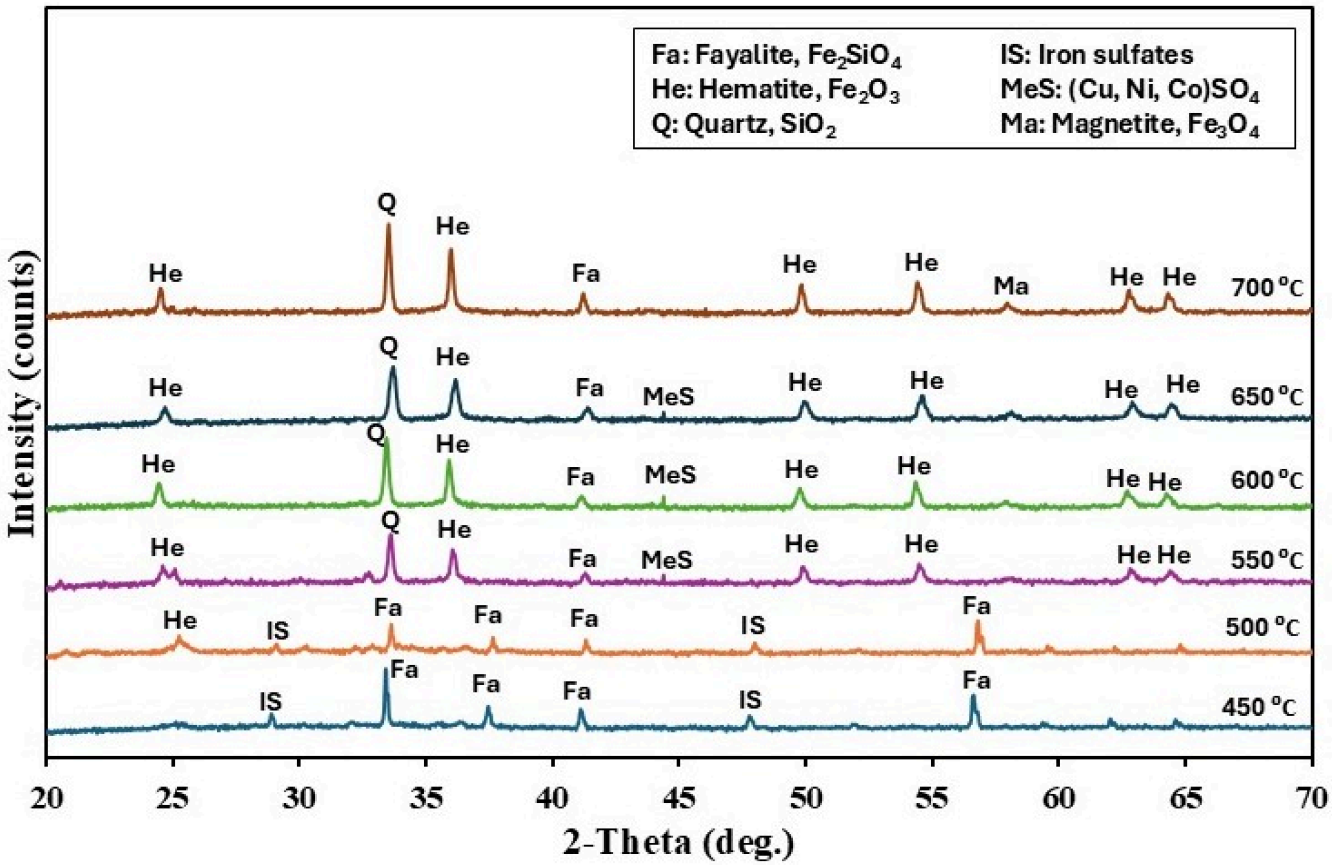


Figure 4. XRD patterns of calcines obtained at different temperatures.

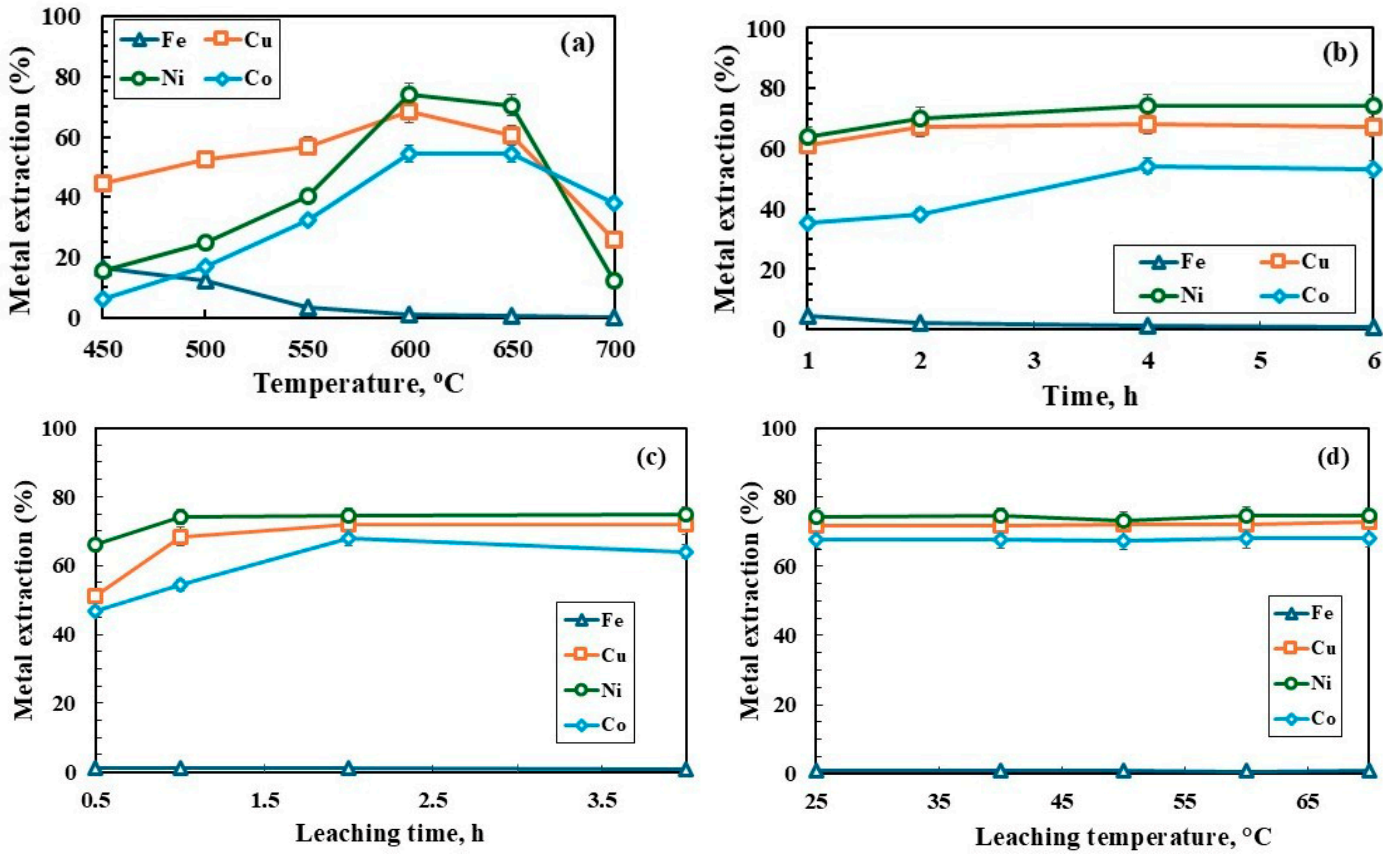


Figure 5. *Cont.*

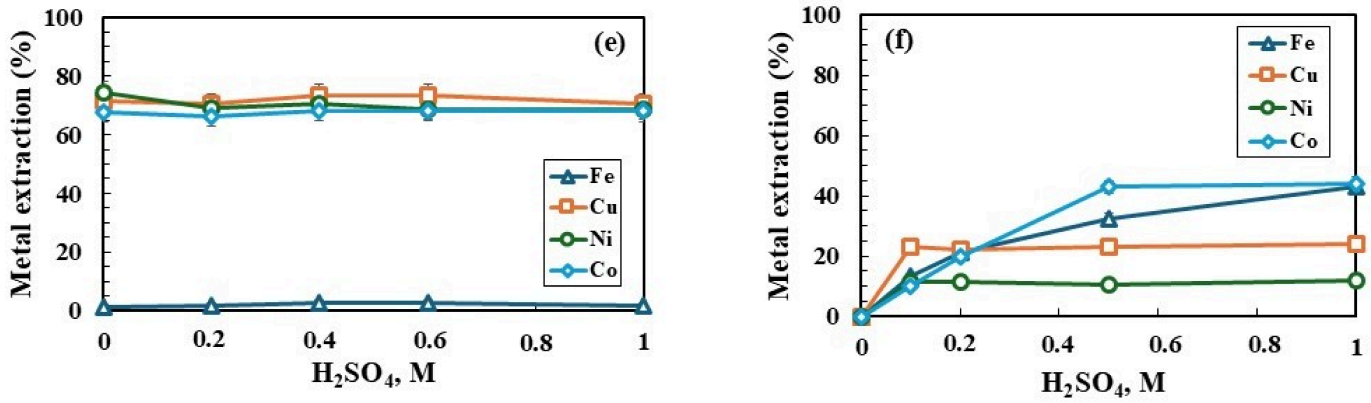


Figure 5. Metal extraction under different roasting and leaching parameters: (**a**) the effect of roasting temperature on the extraction of metals; (**b**) the effect of roasting time on the extraction of metals; (**c**) the effect of leaching time on the extraction of metals; (**d**) the effect of leaching temperature on the extraction of metals; (**e**) the effect of leaching solution on the extraction of metals; (**f**) the effect of leaching solution on the extraction of metals from raw slag (S:T = 1:1, pulp density 10%, shaking speed 180 rpm).

The decrease in Cu, Ni, and Co dissolution is attributed to the thermal instability and partial decomposition of metal sulfates, as well as the formation of less water-soluble oxide phases. This interpretation is consistent with the XRD pattern, where hematite becomes dominant at 700 °C, and with the lower extraction efficiencies observed during subsequent water leaching. Additionally, iron extraction decreased sharply with increasing temperature: from 5.2% at 450 °C to nearly 0% at 700 °C. This behavior is consistent with the known thermal instability and decomposition of ferric sulfate at elevated temperatures, as previously reported by Siriwardane et al. [43].

2.2.2. Effect of Roasting Time

The effect of roasting time on metal extraction was investigated at a fixed temperature of 600 °C using the same slag-to-tailings mass ratio applied in the temperature-dependent experiments. All subsequent leaching parameters were maintained constant. The roasting duration was varied between 1 and 6 h to evaluate the progression of sulfation reactions and their impact on metal recoveries.

As shown in Figure 5b, sulfation reactions initiated rapidly within the first hour of roasting, indicating effective activation of pyrite at 600 °C. Nevertheless, the extraction efficiencies of nickel, copper, and cobalt continued to increase with prolonged roasting time, reflecting the gradual conversion of metal-bearing phases into water-soluble sulfates. Maximum extraction yields were attained after 4 h of roasting, reaching 74.1% for Ni, 68.3% for Cu, and 54.3% for Co. Beyond this duration, no significant improvement in metal extraction was observed, suggesting that sulfation reactions had reached completion or equilibrium under the applied conditions.

Accordingly, a roasting time of 4 h was identified as optimal for maximizing the extraction of valuable metals while avoiding unnecessary energy consumption or potential sulfate decomposition at extended durations.

2.3. Leaching

2.3.1. Effect of Leaching Time

The effect of leaching time on metal extraction was evaluated under optimal roasting conditions, and the results are presented in Figure 5c. The extraction efficiencies of Cu and Co increased markedly with increasing leaching time, reaching 71.8% and 67.8%, respectively, as the leaching duration was extended from 0.5 to 2 h, indicating time-dependent

dissolution behavior. In contrast, nickel extraction showed only a marginal increase, attaining 74.4% over the same period, which suggests limited leaching selectivity for Ni under the applied water-leaching conditions. Prolonging the leaching time beyond 2 h did not result in any significant further improvement in the extraction of any of the investigated metals.

2.3.2. Effect of Leaching Temperature

Figure 5d presents the dissolution profiles of the target metals as a function of leaching temperature, with all other parameters, including a leaching time of 2 h, kept constant as in previous experiments. The results indicate that increasing the leaching temperature had no significant effect on the dissolution behavior of the metals under the given conditions. The negligible impact of leaching temperature on metal dissolution suggests that the process is either kinetically controlled at lower temperatures or limited by other factors such as passivation or solubility constraints. This indicates that the dissolution of sulfated metal species ($NiSO_4$, $CuSO_4$, and $CoSO_4$) is likely rapid and thermodynamically favorable at ambient conditions due to their high solubility in water [44].

2.3.3. Effect of Leaching Solution

To evaluate the effect of leaching medium on metal extraction, sulfuric acid solutions of varying concentrations were used as an alternative to distilled water. The extraction yields obtained at 25 °C are shown in Figure 5e. For the sulfated calcines, no significant differences were observed in the extraction efficiencies of Cu, Ni, and Co across the range of acid concentrations tested, nor compared to leaching with distilled water. This indicates that these metals were already present as highly water-soluble sulfates, formed during sulfation roasting. As such, the addition of acid did not enhance dissolution further. In contrast, the extraction of Fe showed a slight increase with acid concentration, reaching a maximum of 2.5% at 0.4 M H_2SO_4. Thus, increasing the sulfuric acid concentration in the leaching solution does not lead to improved metal recovery, which is consistent with the findings reported by Wan et al. [22].

Figure 5f illustrates the effect of sulfuric acid concentration on the leaching behavior of raw slag. The extraction efficiencies of Fe, Cu, Ni, and Co were evaluated over a sulfuric acid concentration range of 0–1.0 M under identical leaching conditions. As illustrated, the extraction ratios of copper and nickel remain nearly constant across the investigated acid concentration range, indicating limited sensitivity to increasing acidity. This behavior confirms that Cu and Ni are predominantly present in sulfide forms within the raw slag, which show poor solubility in non-oxidizing sulfuric acid media. In contrast, the extraction efficiencies of iron and cobalt increase steadily with increasing sulfuric acid concentration. This trend is characteristic of metals present in oxide or silicate-associated forms, which dissolve readily via acid–oxide reactions.

Overall, the distinct leaching ratios highlight the mineralogical heterogeneity of the raw slag, where Cu and Ni are largely immobilized in acid-resistant sulfide phases, whereas Fe and Co are present in more acid-reactive oxide forms. These findings further justify the need for a sulfation roasting pre-treatment to transform refractory sulfide and silicate phases into soluble species, thereby improving the subsequent recovery of valuable metals.

2.4. Effect of Slag/Tailing Ratio

Following the determination of optimal roasting and leaching conditions, the effect of varying the slag-to-tailings (S:T) mass ratio on metal extraction was examined. Ratios of S:T = 2:1 and S:T = 1:2 were tested and yielded comparatively lower extraction efficiencies for valuable metals. As presented in Figure 6, average Cu and Ni extraction rates were approximately 56% and 50%, respectively, for both cases. In the case of cobalt, extraction was particularly low at 42% for the 2:1 ratio but improved significantly at the 1:2 ratio, approaching

the extraction levels observed under the optimal 1:1 condition. From a stoichiometric perspective, the slag-to-tailings ratio controls the balance between the amount of metal-bearing phases requiring sulfation and the sulfur-bearing gases generated from pyrite oxidation. When the tailings dosage is insufficient (S:T = 2:1), the generation of SO_2/SO_3 is limited, leading to incomplete conversion of Cu-, Ni-, and Co-bearing phases into water-soluble sulfates. Conversely, excessive tailings addition (S:T = 1:2) may increase sulfur oxide generation beyond the amount required for sulfation and disturb the local oxidation–sulfation balance. Under such conditions, excessive sulfur-bearing species and iron-rich reaction products may favor the formation of less soluble phases or promote encapsulation of target metals within newly formed iron oxide/silicate matrices. Therefore, the optimal S:T = 1:1 ratio reflects a balanced supply of sulfur-bearing gases relative to the metal-bearing slag, enabling effective sulfate formation while minimizing unfavorable secondary reactions.

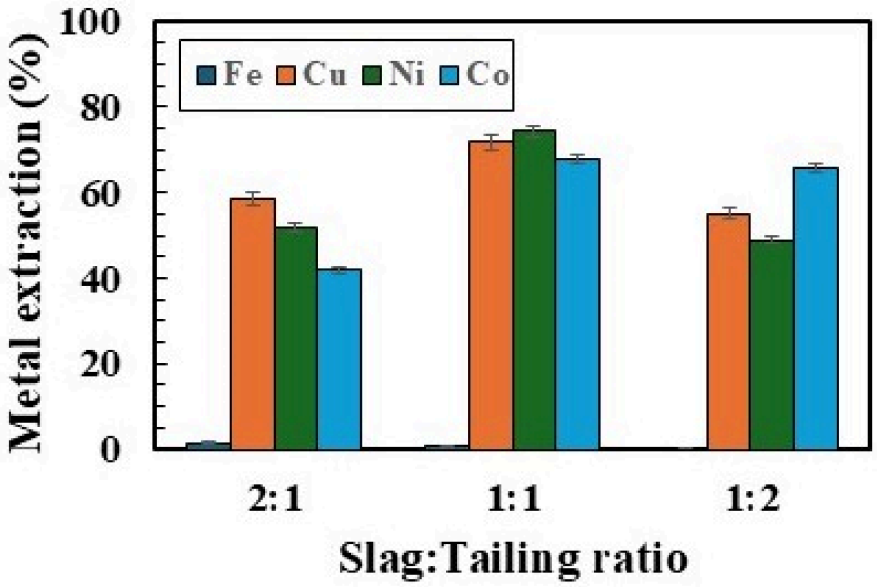


Figure 6. Effect of the Slag:Tailings ratio on the metal extraction (roasting time 4 h, roasting temperature 600 °C, leaching time 2 h, leaching temperature 25 °C, pulp density 10%, shaking speed 180 rpm).

2.5. Effect of SMBS Addition

The addition of sodium-based salts, particularly sulfates, has been widely reported to enhance the kinetics of sulfation roasting by facilitating sulfate formation and improving metal solubility. Previous studies by Yu et al. [45], Li et al. [46], Sun et al. [41], and Wan et al. [22] demonstrated that the incorporation of sodium sulfate (Na_2SO_4) during roasting, followed by water leaching, significantly improves metal recovery from a range of metallurgical materials.

In the present study, the effect of an alternative sodium salt—sodium metabisulfite ($Na_2S_2O_5$)—was systematically investigated under fixed optimal roasting and leaching conditions.

The addition of SMBS during roasting markedly enhanced metal extraction, as shown in Figure 7. The improved extraction of Cu, Ni, and Co after SMBS addition indicates that SMBS acts primarily as a sulfation promoter rather than the principal sulfur source. The pyrite-rich flotation tailings provide the majority of sulfur-bearing gases required for sulfation, whereas SMBS likely enhances the local SO_2/SO_3 atmosphere and promotes sulfate formation and stability. The highest extraction efficiencies were achieved with 30 wt% SMBS relative to the total mass of the slag–tailing mixture, yielding 85.5% Cu, 81.6% Ni, and 87.1% Co. The substantial improvement in cobalt extraction is consistent

with previous reports by Ntakamutshi et al. [47] and Tshipeng et al. [48], who highlighted the effectiveness of SMBS in enhancing cobalt sulfation.

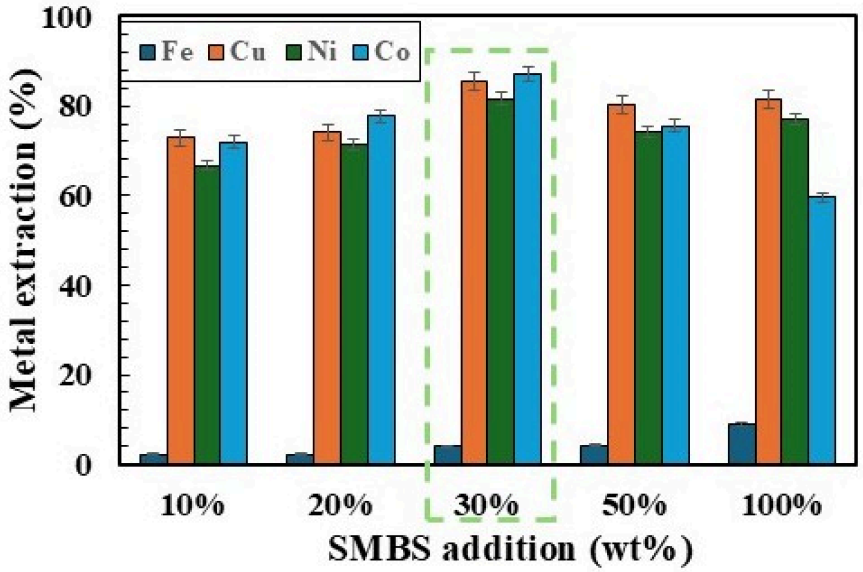


Figure 7. Effect of SMBS addition on the metal extraction. (S:T = 1:1, roasting time 4 h, roasting temperature 600 °C, leaching time 2 h, leaching temperature 25 °C, pulp density 10%, shaking speed 180 rpm).

2.6. Effect of Na_2SO_4 Addition

A comparison of the effects of SMBS and sodium sulfate (Na_2SO_4) additions during roasting is presented in Figure 8. Under identical conditions, the extraction efficiencies of Cu and Ni are higher in the presence of SMBS than with sodium sulfate, while cobalt extraction shows a significant enhancement, increasing by approximately 16% with SMBS addition.

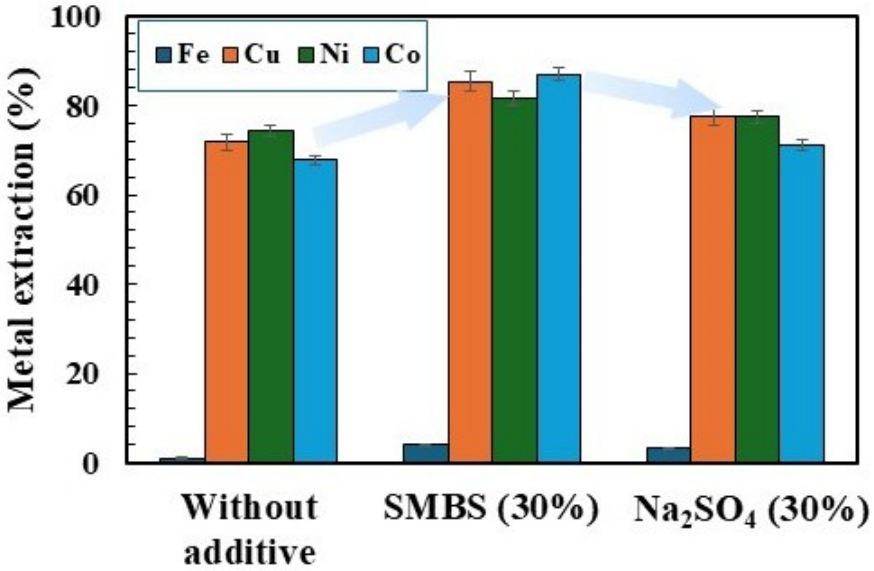


Figure 8. Effect of Na_2SO_4 on the metal extraction and comparison with the effect of SMBS.

This enhanced performance is attributed to the more aggressive sulfating environment generated by SMBS. Figure 9 shows the XRD pattern of the sample roasted with SMBS, where a diffraction peak corresponding to the eutectic sulfate phase $Na_2Me(SO_4)_2$ is observed.

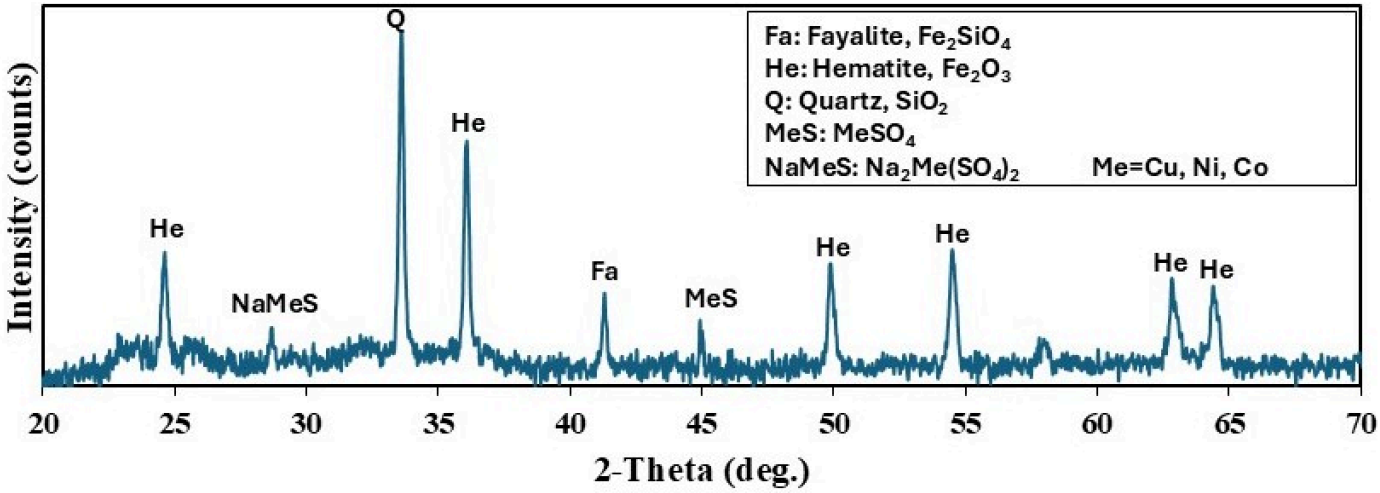


Figure 9. XRD pattern of the sample roasted with SMBS.

Unlike Na_2SO_4, which releases SO_4^{2-} ions, $Na_2S_2O_5$ thermally decomposes to release SO_2, forming a more reactive sulfating atmosphere. The presence of gaseous SO_2, in particular, facilitates the formation of $CoSO_4$ according to Reaction (R14):

$$CoO + SO_2 + 0.5O_2 \rightarrow CoSO_4 \quad \text{(R14)}$$

This direct sulfation pathway is more effective under the thermal conditions applied, thereby improving cobalt recovery. The findings suggest that SMBS, due to its decomposition behavior and gas-phase reactivity, offers a more favorable roasting environment for the sulfation of cobalt compared to Na_2SO_4.

SEM micrographs illustrating the morphological evolution of the slag during roasting with tailings and SMBS, as well as after subsequent water leaching, are displayed in Figure 10. Figure 10a (raw slag) displays relatively dense, angular particles with smooth and compact surfaces, characteristic of fayalite-based smelter slag. The limited surface roughness and low porosity indicate a structurally stable silicate matrix, which is consistent with the refractory nature of the raw slag and its poor leachability.

After roasting with tailings (Figure 10b), the slag particles exhibit surface cracking, partial fragmentation, and increased roughness. These changes indicate the fayalite decomposition and sulfide oxidation, leading to the disruption of the original compact slag structure. However, the particles largely retain their dense core morphology, suggesting that sulfation reactions remain kinetically limited under these conditions.

In contrast, the slag roasted with both tailings and SMBS (Figure 10c) shows a markedly more porous, irregular, and fragmented morphology. The particle surfaces are covered with fine granular features and micro-scale protrusions, indicative of intensive solid–gas reactions and sulfate formation. This pronounced structural breakdown reflects the enhanced sulfation kinetics induced by SMBS, which promotes early sulfur oxide release and facilitates deeper penetration of reactive species into the slag particles.

The leaching residue (Figure 10d) presents a highly porous and friable structure, composed of loosely aggregated fine particles. The absence of smooth surfaces suggests that water-soluble sulfate phases have been effectively dissolved during leaching, leaving behind a porous framework dominated by iron oxides and residual silicate phases. This morphology is consistent with the high extraction efficiencies observed for Cu, Ni, and Co after SMBS-assisted roasting.

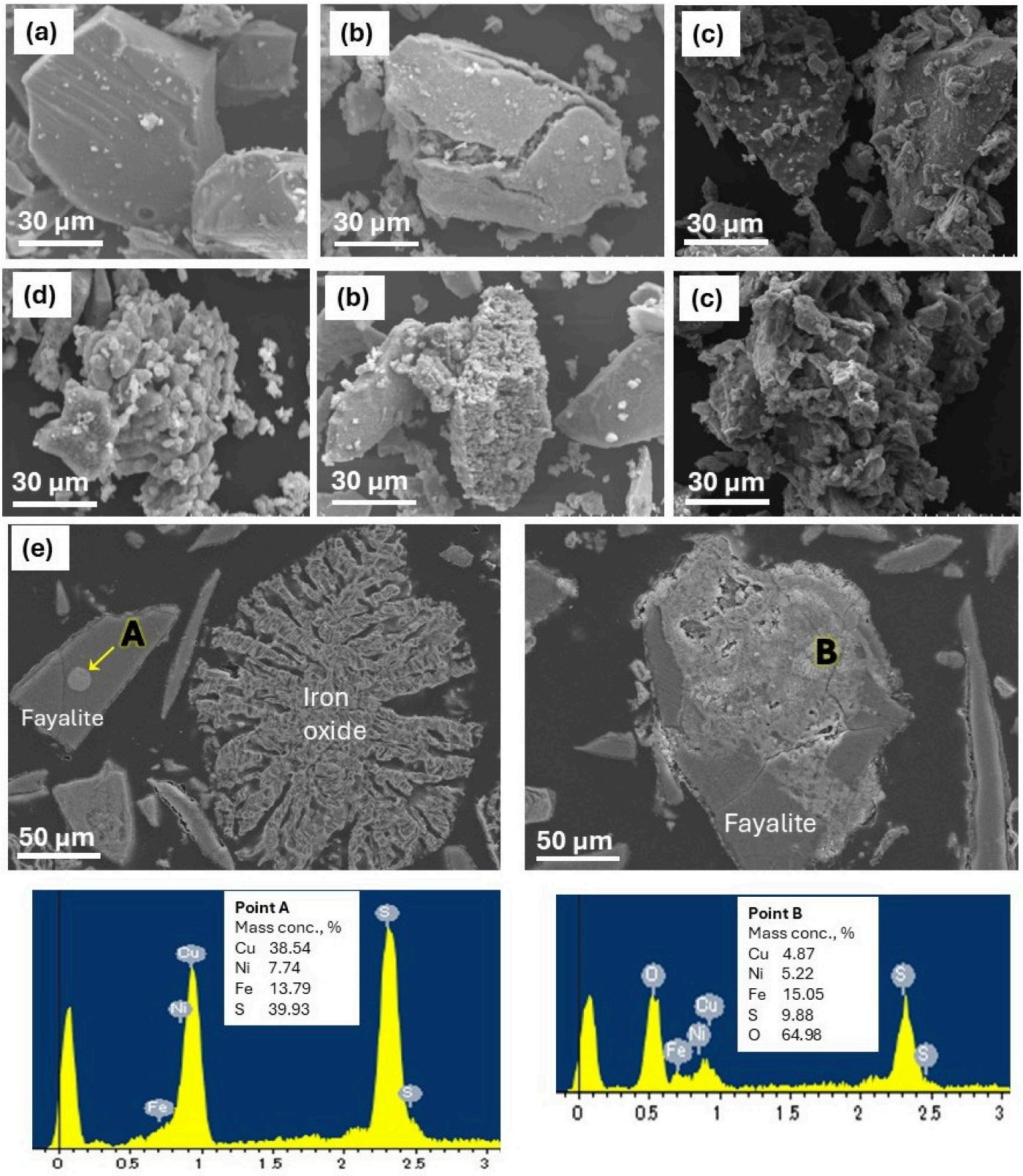


Figure 10. SEM micrographs of (**a**) slag sample, (**b**) slag roasted with tailings, (**c**) slag roasted with tailings and SMBS, (**d**) leach residue, and (**e**) cross-sectional image of roasted slag with tailings.

Figure 11 presents the SEM image and corresponding EDS elemental maps of the cross-section of the roasted slag–tailings–SMBS sample. The image reveals a heterogeneous microstructure consisting of dense primary particles embedded within a finer matrix, indicating partial phase transformation and redistribution during roasting. SEM–EDS

mapping confirms that the addition of SMBS promotes the redistribution of sulfur into oxidized sulfate phases and facilitates the dispersion and partial sulfation of Cu- and Ni-bearing phases, providing microstructural evidence for enhanced sulfation roasting. The point EDS analyses (Spectrums 1 and 2) further confirm the coexistence of O, S, Na, Fe, Cu, and Ni within the same region, supporting the formation of complex oxide–sulfate assemblages rather than simple sulfide phases.

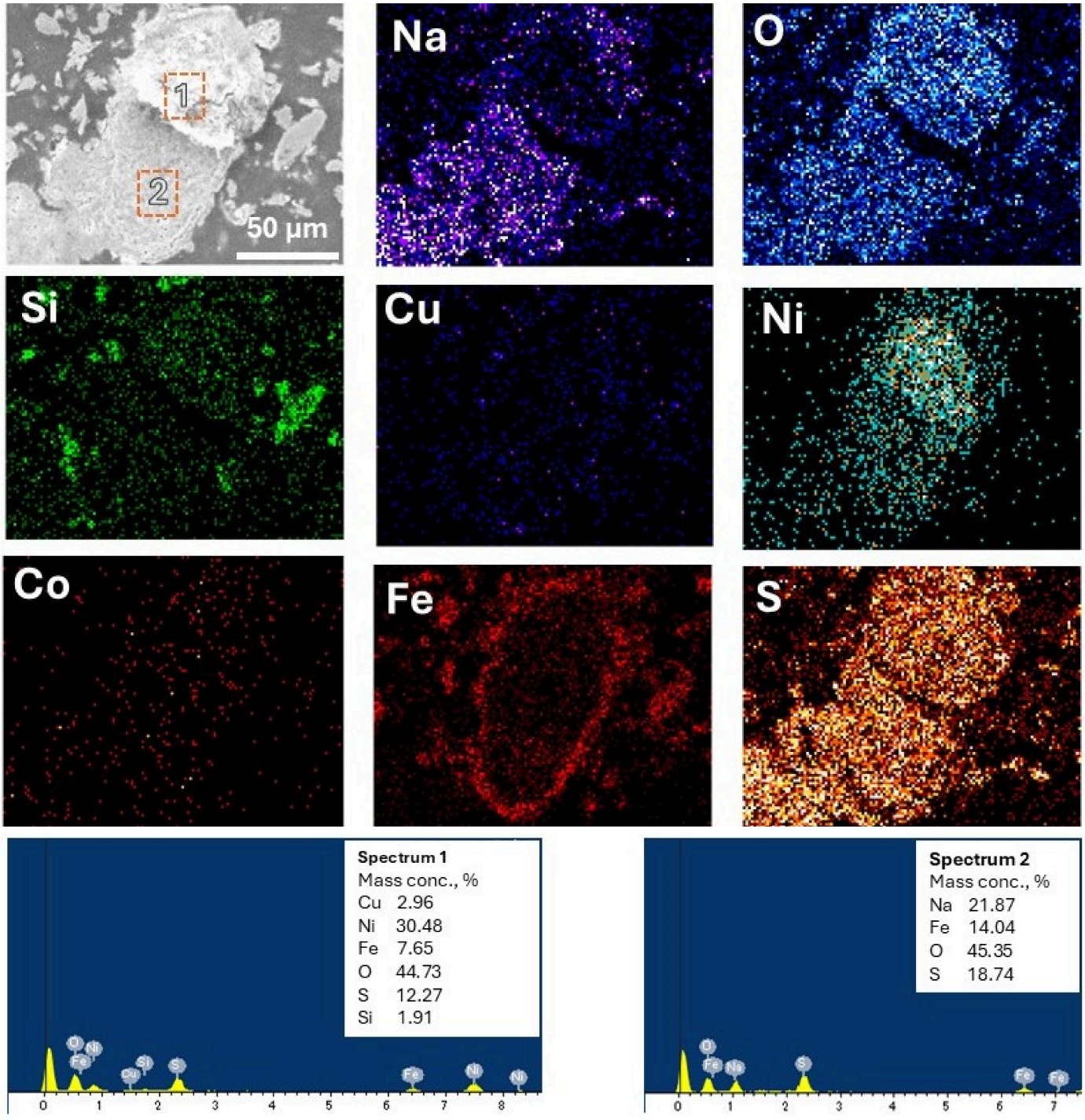


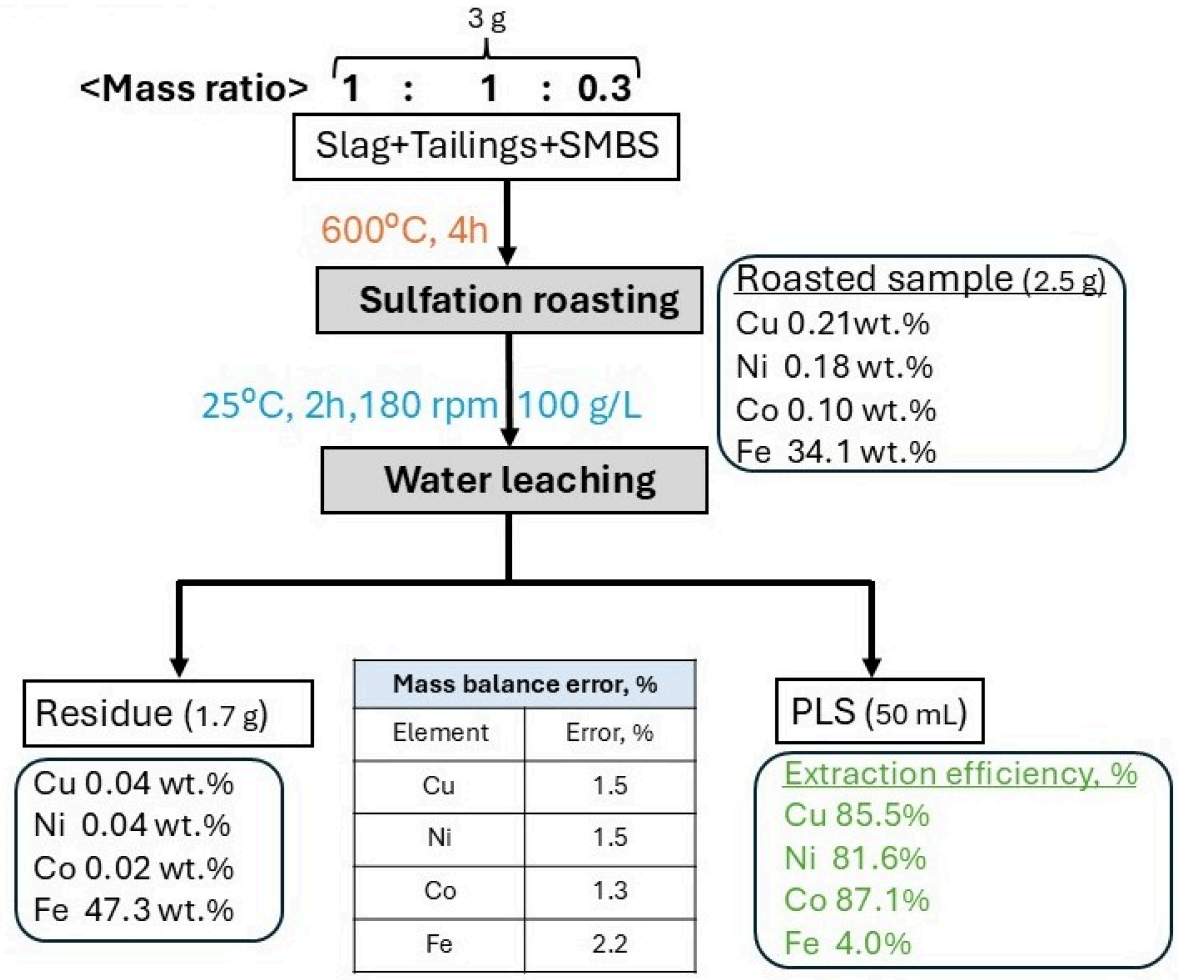
Figure 11. SEM-EDS images showing the elemental mapping of the SMBS-assisted roasting sample.

Although significant improvements in metal extraction were achieved, the overall recoveries remained within a moderate range of 80–90%. This limitation can be attributed to the partial encapsulation of matte droplets within the primary crystalline phase, namely

fayalite, where they occur as ferrite- and silicate-associated phases (Figure 10e). Such incorporation hinders their complete conversion into soluble sulfates under the investigated conditions [21,49].

2.7. Mass Balance and Characterization of Leach Residue

Under the optimum roasting and leaching conditions, the mass balance of Cu, Ni, Co, and Fe was evaluated and is summarized in Figure 12. The mass balance closure errors for all investigated elements were below 2.5%, indicating good agreement between the metal contents in the roasted sample, pregnant leach solution (PLS), and final leach residue and confirming the reliability of the analytical results.



Mass balance error, %	
Element	Error, %
Cu	1.5
Ni	1.5
Co	1.3
Fe	2.2

Figure 12. Mass balance flow diagram for Cu, Ni, Co, and Fe under the optimum roasting and leaching conditions.

As shown in Figure 12, the majority of Cu, Ni, and Co were transferred into the PLS. Such selective behavior is advantageous for downstream processing because it minimizes the dissolution of iron impurities and may simplify subsequent purification and recovery of Cu, Ni, and Co from the leach solution.

The chemical composition of the final leach residue is presented in Table 3. The residue contained only 0.04 wt.% Cu, 0.04 wt.% Ni, and 0.02 wt.% Co, confirming that most of the valuable metals had been converted into water-soluble sulfate phases during roasting and dissolved during water leaching.

Table 3. Chemical composition of the leach residue (wt.%).

Sample	Cu	Ni	Co	S	Fe_2O_3	SiO_2	Al_2O_3
Leach residue	0.04	0.04	0.02	0.71	72.14	18.11	3.39

2.8. FTIR and Thermogravimetric Analysis

Figure 13 presents the FTIR spectra of the roasted slag–tailings system with and without SMBS, as well as the leaching residue obtained after water leaching. The spectra provide clear evidence of phase evolution and confirm the role of SMBS in enhancing sulfation during roasting.

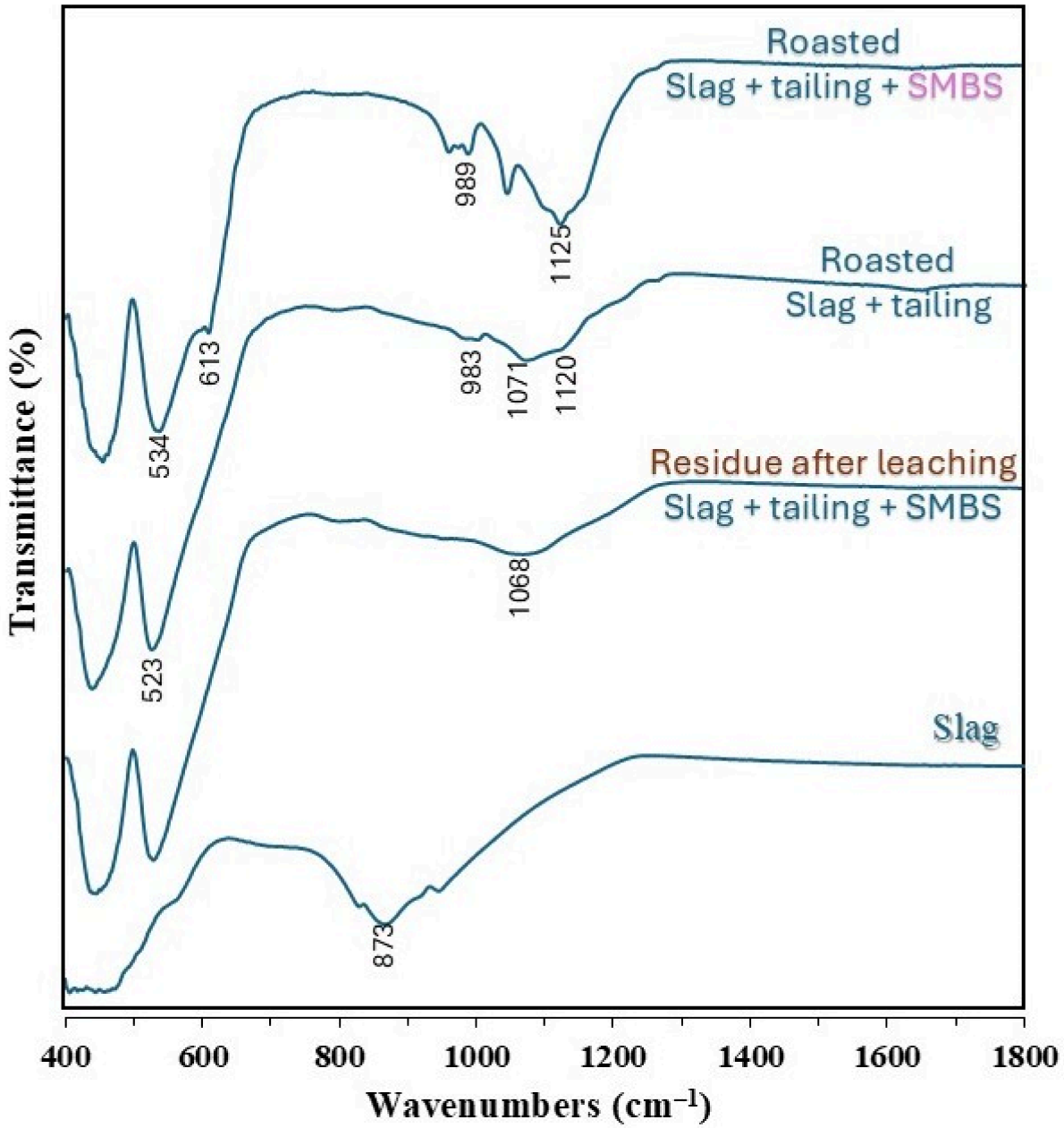


Figure 13. FTIR spectrum of the calcines and residue obtained after leaching.

In the spectrum of the roasted slag–tailings–SMBS sample, pronounced absorption bands appear at approximately 1125, 989, and 613 cm^{-1}, which are characteristic of SO_4^{2-} vibrations [50]. These sulfate-related bands are either weak or barely detectable in the

spectrum of the roasted slag–tailings sample without SMBS, indicating that sulfation is significantly enhanced by the addition of SMBS during roasting.

Bands observed in the region of 1060–1070 cm^{-1} are also attributed to Si–O stretching vibrations, indicating the presence of silicate phases such as quartz or residual fayalite. The persistence of these bands suggests that, although fayalite decomposition occurs during roasting, silicate frameworks remain in the calcined material [11].

In the low-wavenumber region around 520–540 cm^{-1}, absorption bands associated with Fe–O vibrations are observed, confirming the formation of iron oxide phases, such as hematite, as a result of fayalite decomposition and oxidation during roasting [51]. These bands are present in both roasted samples, indicating that iron oxidation proceeds regardless of SMBS addition.

The FTIR spectrum of the leaching residue obtained from the slag–tailings–SMBS system shows a marked attenuation or disappearance of sulfate bands, while silicate (Si–O) and Fe–O bands remain prominent. This observation indicates that most metal sulfate species formed during roasting are readily dissolved during water leaching, leaving behind a residue dominated by iron oxides and silicate phases.

Overall, the FTIR results demonstrate that the addition of SMBS significantly promotes the formation of sulfate species during roasting, as evidenced by the intensified SO_4^{2-} bands. The subsequent disappearance of these bands in the leaching residue confirms the high solubility of the formed metal sulfates, providing direct spectroscopic evidence for the enhanced sulfation and improved extraction of valuable metals in the SMBS-assisted roasting process.

Figure 14 presents the TG–DTA curves of the slag–tailings (a) and slag–tailings–SMBS (b) mixtures recorded under an inert argon atmosphere at a heating rate of 10 °C·min^{-1}.

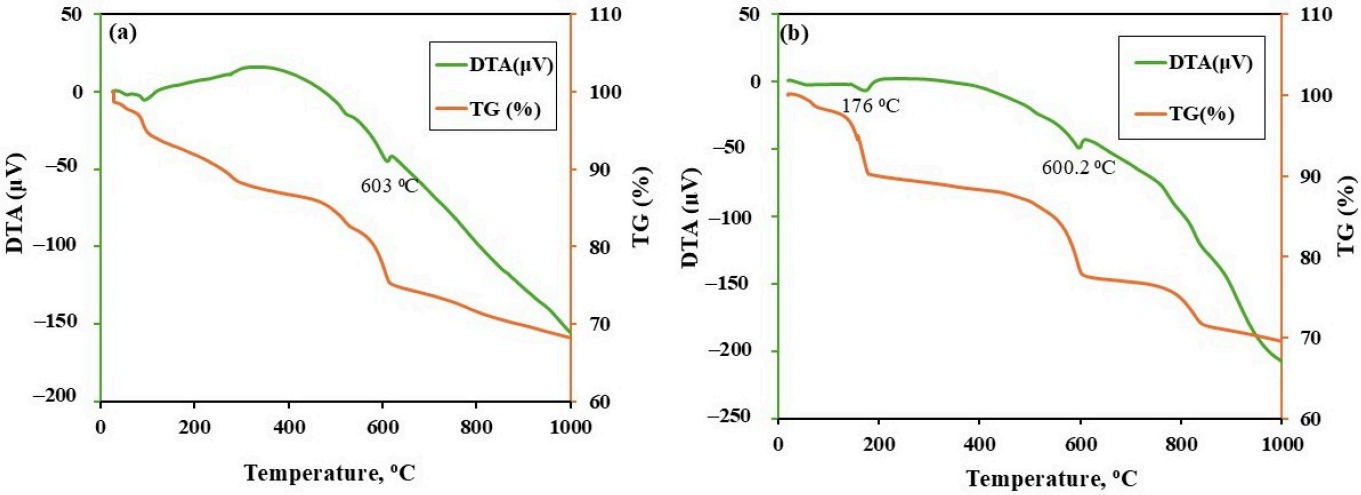


Figure 14. TG-DTA curves of the slag-tailing (**a**) and slag-tailing-SMBS (**b**).

For the slag–tailings mixture (Figure 14a), the TG curve shows a gradual mass decrease over the entire temperature range, reaching a total mass loss of approximately 30–32% at 1000 °C. No significant mass gain is observed, indicating that under inert conditions sulfur volatilization dominates over any mass-increasing reactions.

Below approximately 250–300 °C, the mass loss is limited (only a few percent), which can be attributed to the removal of physically adsorbed moisture and minor volatile species. In this region, the DTA signal remains close to baseline, confirming the absence of major chemical reactions.

A notable acceleration in mass loss occurs around 500–650 °C, where the TG curve exhibits a pronounced downward slope. At approximately 600 °C, the remaining mass

decreases to about 75% of the initial sample mass, corresponding to a mass loss of 25%. This temperature range coincides with a clear endothermic trend in the DTA curve and is attributed to the thermal decomposition and transformation of pyrite, accompanied by the release of sulfur-bearing gaseous species. This stage represents the primary sulfur-release window for the slag–pyrite system under an inert atmosphere.

Above 650 °C, the TG curve continues to decline gradually, reaching its final value at 1000 °C. This behavior reflects continued sulfur volatilization and solid-state rearrangement of Fe–S phases, as well as interactions between iron sulfides and the fayalite-based slag matrix.

In contrast, the slag–tailings–SMBS mixture (Figure 14b) shows a distinct early mass-loss step at low temperature, followed by high-temperature behavior similar to that of the slag–pyrite system.

A clear mass loss of approximately 10% occurs below 200 °C, which is accompanied by a pronounced endothermic peak in the DTA curve. This low-temperature event is attributed to the thermal decomposition of sodium metabisulfite, resulting in the release of sulfur-containing gaseous species and the formation of sodium sulfite/sulfate phases. This early sulfur release is absent in the slag–pyrite system and represents a key mechanistic difference introduced by SMBS.

In the intermediate temperature range (300–450 °C), the TG curve shows only minor additional mass change, indicating relative thermal stability of the decomposition products formed at lower temperature. Similar to the slag–pyrite system, a major mass-loss region is observed between 500 and 600 °C. At approximately 600 °C, the remaining mass is about 78%, corresponding to a mass loss of 22%, which is comparable to that of the slag–pyrite system. This confirms that the high-temperature sulfur release associated with pyrite decomposition remains operative even in the presence of SMBS. At temperatures above 850 °C, a gradual mass decrease up to 1000 °C is observed in both systems, reaching a final mass loss of approximately 32%.

Overall, the TG–DTA results demonstrate that the addition of SMBS broadens the effective sulfur-release temperature window by introducing an early low-temperature decomposition step while preserving the high-temperature sulfur contribution from pyrite. Although these measurements were conducted under inert conditions, the observed thermal behavior provides strong mechanistic support for the enhanced sulfation roasting performance observed under oxidizing conditions. In particular, the early release of sulfur species from SMBS is expected to facilitate SO_2/SO_3 generation at lower temperatures, thereby accelerating sulfation kinetics and promoting the formation of water-soluble metal sulfates during roasting.

2.9. Industrial Implications and Limitations

The extraction of Cu, Ni, and Co into the pregnant leach solution represents an intermediate step toward final metal recovery. Depending on the composition of the leachate, several downstream processing routes may be employed, including selective precipitation, solvent extraction, ion exchange, and electrowinning [52]. Copper may be preferentially recovered by sulfide precipitation or solvent extraction-electrowinning, whereas Ni and Co can subsequently be separated using solvent extraction systems or selective precipitation techniques [53,54]. The relatively low dissolution of Fe observed in the present study is advantageous because it minimizes impurity removal requirements and may simplify downstream processing. However, the simultaneous presence of Cu, Ni, and Co in solution may still pose challenges for selective separation, and further studies are required to optimize metal recovery and purification from the pregnant leach solution.

Although the proposed process operates at a relatively low roasting temperature (600 °C) compared with many conventional pyrometallurgical reduction routes, the roasting time (4 h) and the addition of 30 wt.% SMBS may influence the overall process economics and should be considered during scale-up. Furthermore, pyrite oxidation and SMBS decomposition may generate SO_2 and SO_3 gases, necessitating appropriate gas collection and treatment systems in industrial applications. The process may also generate sodium-containing residues and pregnant leach solutions that require appropriate downstream treatment and management.

From an industrial perspective, the proposed process simultaneously valorizes two metallurgical waste streams and could potentially be integrated with existing smelting operations or legacy tailings reprocessing projects, where flotation tailings and copper smelter slags are already available on site. Nevertheless, further studies, including techno-economic assessment, life cycle analysis, sulfur mass balance, and pilot-scale investigations, are required before the environmental sustainability and industrial feasibility of the proposed process can be fully established.

3. Materials and Methods

3.1. Materials

The slag and tailings samples used in this research were obtained from a copper-nickel smelter in Botswana. The reprocessing of tailings dam materials is driven by both environmental and economic imperatives: residual metal grades in legacy tailings can approach or even exceed those of freshly mined deposits, making such materials attractive targets for secondary recovery [55]. Under the thermal conditions of sulfation roasting, iron sulfide minerals within the tailings are oxidized to relatively insoluble ferric oxide phases, causing iron to partition into the solid residue upon filtration rather than reporting to the leach solution. An additional benefit of this co-treatment approach is that target metals hosted within the tailings can be co-recovered alongside those from the slag, improving aggregate metal yield while reducing the environmental burden of both waste streams [56].

XRD analysis of the slag (Figure 15a) confirmed fayalite as the dominant mineralogical phase, whereas pyrite was identified as the major phase in the flotation tailings (Figure 15b). SEM-EDS elemental mapping of the granulated material is shown in Figure 16, revealing that copper and nickel occur as sulfide-form matte droplets dispersed throughout the silicate matrix, whereas cobalt is distributed relatively uniformly within the fayalite phase, indicating its predominance in an oxide form. This mineralogical partitioning is well established for copper smelter slags, in which the higher oxygen affinity of cobalt causes it to report to the oxide phase while Ni and Cu are stabilized as sulfides [57,58].

XRF spectrometry was used to determine the elemental composition of the samples. The chemical compositions of smelter slag and the tailings are shown in Table 4.

Table 4. Chemical composition of the samples (wt.%).

Samples	Cu	Ni	Co	Fe	S	Si	Al
Slag	0.32	0.35	0.17	37.51	0.81	13.24	3.30
Tailings	0.11	0.09	0.01	38.62	41.14	1.31	1.86

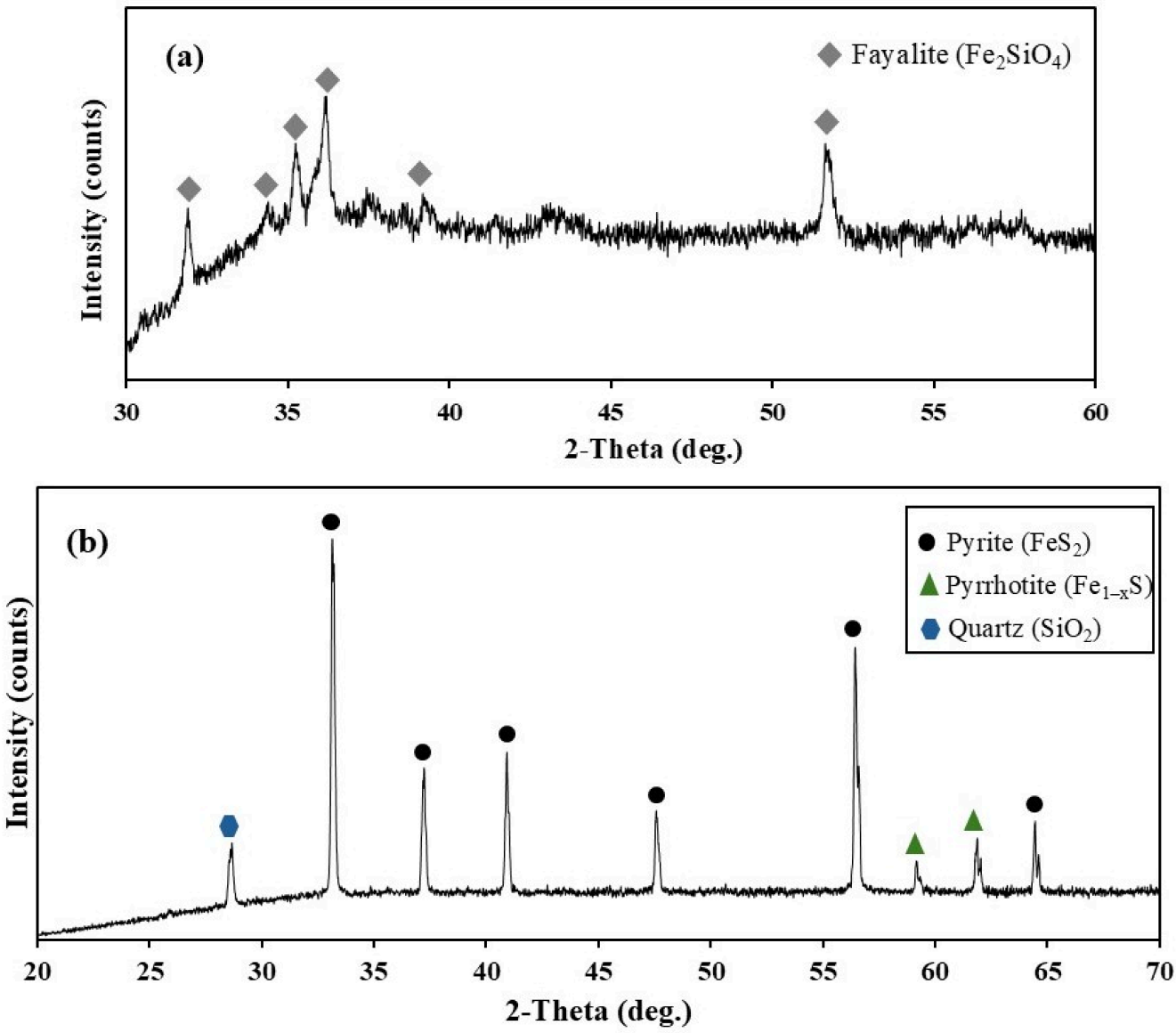


Figure 15. XRD patterns of the smelter slag (**a**) and flotation tailings (**b**).

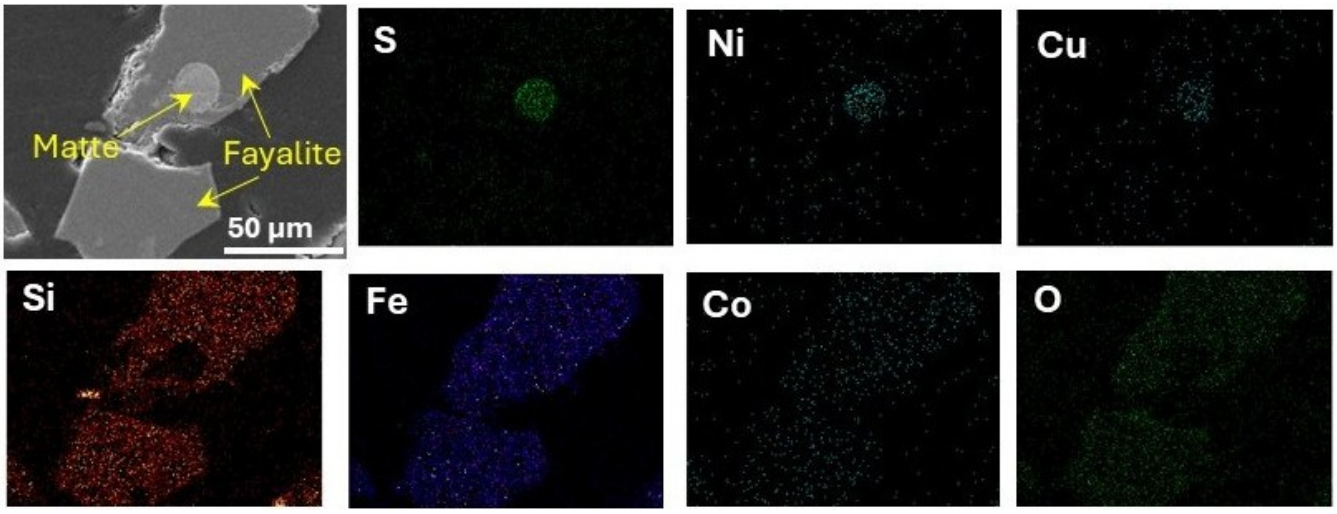


Figure 16. SEM image and elemental mapping of the slag sample.

3.2. Experimental Method

The proposed utilization method for smelter slag and tailings is illustrated in Figure 17. The process consists of two main stages: sulfation roasting and subsequent leaching. Sulfation roasting experiments were carried out in a muffle furnace using a ceramic boat loaded with a 3 g sample. After completion of the roasting step, the samples were allowed to cool to room temperature and were then subjected to water leaching to recover the valuable metals into the solution followed by solid–liquid separation. Distilled water used in all experiments was produced using a water purification system (Auto Still Yamato WG250, Yamato, Tokyo, Japan). Through enhanced roasting, the slag structure is destroyed, releasing the entrapped Cu, Ni, and Co sulfides and oxides, which are then sulfated for easy dissolution in water. The insoluble Fe(Ill) oxide is then easily separated from the leaching solution. The sample mass was measured before and after roasting in each experiment to evaluate weight changes associated with thermal decomposition and sulfation reactions. The amount of SMBS (reagent grade 97% purity, Sigma-Aldrich, Buchs, Switzerland) added under the optimum conditions was 0.69 g, corresponding to 30 wt.% of the slag-tailings mixture. The roasting process is followed by water leaching to recover valuable metals. In each leaching test, 2.5 g of the product sample was treated in a beaker containing 25 mL of distilled water. The beaker was placed in a thermostatically controlled water bath shaker to maintain a constant leaching temperature. The pulp density and stirring speed were kept constant at 100 g/L and 180 rpm, respectively. Then the slurry was filtered, and both PLS and residue were analyzed. The average values of the dissolved metals were utilized to calculate the leaching rate after the leaching tests. All leaching experiments were performed in triplicate. The reported values represent the mean of three independent experiments, and the error bars indicate the corresponding standard deviations. Each roasting condition was conducted once due to the time- and energy-intensive nature of the roasting procedure, and the resulting calcines were subsequently subjected to triplicate leaching experiments.

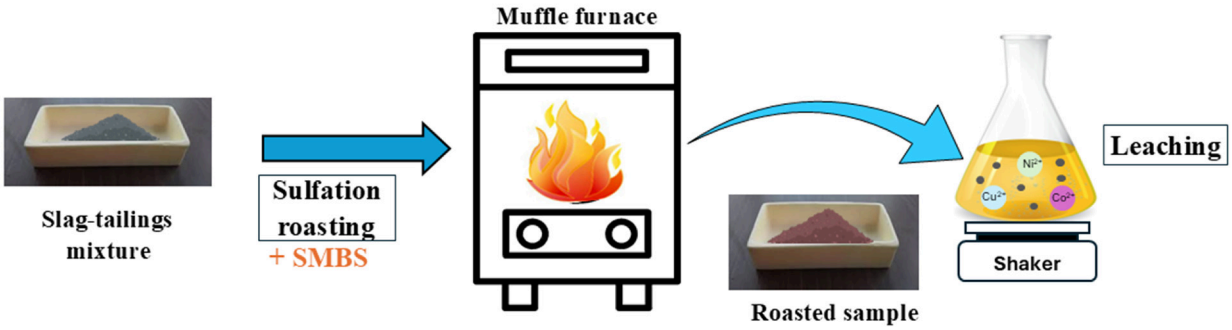


Figure 17. Schematic diagram of slag utilization.

The leaching rate is calculated according to Equation (2):

$$R_M(\%) = \frac{C_L \cdot V_L}{C_F \cdot M_F} \times 100 \quad (2)$$

where C_L and C_F are the concentrations of metals in the PLS (mg/L) and feed (mg/g), respectively. V_L is the volume of PLS (L) and M_F is the dry mass of the feed (g). The reported values represent metal extraction into solution and not the final recovery after downstream purification.

3.3. Analysis

X-ray fluorescence (XRF) spectrometry (Rigaku ZSX Primus II, Rigaku, Akishima-shi, Japan) was used to determine the elemental composition of the slag. The mineral composi-

tion phase transition of the materials was investigated using X-ray diffraction (XRD, Miniflex, Rigaku, Akishima-shi, Japan). Additionally, SEM-EDS (Scanning Electron Microscope-Energy Dispersion Spectroscopy SU-70, Hitachi, Tokyo, Japan) was used to characterize the samples. The leaching solutions were analyzed using a 4210 MP-AES (Agilent Technologies Inc., Santa Clara, CA, USA). The finely ground solid samples were analyzed using Fourier Transform Infrared Spectra (Thermo Scientific Nicolet iS50 FT-IR, Thermo Fisher Scientific, Madison, WI, USA) with an iD5 ATR diamond cell. Spectral treatments such as ATR correction data and data collection were performed using the Thermo Scientific OMNIC Spectra 2.0 software. The thermogravimetric (TG) and differential thermal analysis (DTA) were performed with a Rigaku TG-DTA8122 instrument (Rigaku, Akishima-shi, Japan) from 25 °C to 1000 °C in an Ar atmosphere with a heating rate of 10 °C/min.

4. Conclusions

This study evaluated the feasibility of a pyro–hydrometallurgical co-treatment route for the recovery of copper, nickel, and cobalt from copper fayalite slag through sulfation roasting followed by water leaching. The results demonstrate that the proposed process is efficient and represents a promising strategy for the valorization of metallurgical wastes.

The effects of key roasting and leaching variables were systematically investigated. The flotation tailings were successfully employed as a sulfur donor, while sodium metabisulfite (SMBS, $Na_2S_2O_5$) acted as an effective sulfur-oxide promoter, enhancing sulfation kinetics and sulfate formation. Mineralogical characterization confirmed that fayalite is the dominant phase in the copper slag, with valuable metals distributed as sulfides (Cu, Ni) and oxides (Co). The phase transformations during roasting promoted the release of sulfur oxides required for the sulfation of Cu, Ni, and Co species. At the same time, iron was converted into the less soluble hematite phase, thereby suppressing its dissolution during subsequent water leaching.

Thermogravimetric (TG–DTA) analysis showed that SMBS introduced an additional low-temperature sulfur-release stage, which promoted sulfation over a wider temperature range. This finding is consistent with the enhanced metal extraction observed after roasting. FTIR analysis confirmed the formation of sulfate species after roasting and their subsequent dissolution during water leaching, as indicated by the disappearance of characteristic SO_4^{2-} bands in the leaching residues.

Under optimized sulfation roasting conditions (roasting temperature: 600 °C; roasting time: 4 h; slag-to-tailings ratio: 1:1; SMBS addition: 30 wt%), followed by water leaching at 25 °C for 2 h with a pulp density of 10%, extraction efficiencies of 85.5% Cu, 81.6% Ni, and 87.1% Co were achieved, while iron dissolution remained limited to approximately 4%. These results confirm that SMBS plays a crucial catalytic role in promoting sulfation while maintaining high selectivity against iron.

The present study did not evaluate downstream metal recovery, sulfur mass balance, techno-economic feasibility, or life cycle impacts. These aspects should be investigated in future studies to assess the industrial applicability of the proposed process.

Overall, the proposed "waste-on-waste" approach, combining copper slag with flotation tailings, represents a technically viable and potentially sustainable approach for the recovery of valuable metals from copper smelting slags. The methodology may also be extended to other secondary resources containing recoverable base and critical metals.

Author Contributions: Conceptualization, B.G. (Bobur Gayratov), L.L.G. and A.S.; methodology, B.G. (Bobur Gayratov), L.L.G. and A.S.; validation, B.G. (Bobur Gayratov), B.G. and A.S.; formal analysis, B.G. (Bobur Gayratov), B.G. and G.D.; investigation, B.G. (Bobur Gayratov), L.L.G. and A.S.; resources, G.D. and A.S.; data curation, B.G. (Bobur Gayratov), L.L.G. and A.S.; writing—original draft preparation, B.G. (Bobur Gayratov); writing—review and editing, B.G. (Bobur Gayratov), L.L.G.

and A.S.; visualization, B.G. (Bobur Gayratov) and B.G.; supervision, A.S.; project administration, A.S.; funding acquisition, L.L.G. and A.S. All authors have read and agreed to the published version of the manuscript.

Funding: This research received no external funding.

Data Availability Statement: The data presented in this study are available on request from the corresponding author. (The datasets have not been deposited in a public repository but can be provided upon reasonable request.)

Acknowledgments: The authors are grateful for the support provided by Japan International Cooperation Agency (JICA) and Botswana International University of Science & Technology for providing samples.

Conflicts of Interest: The authors declare no conflicts of interest.

References

1. Müller, D.; Groves, D.I.; Santosh, M.; Yang, C. Critical metals: Their applications with emphasis on the clean energy transition. *Geosyst. Geoenviron.* **2025**, *4*, 100310. [CrossRef]
2. Gayratov, B.; Gayratov, B.; Godirilwe, L.L.; Jeon, S.; Saynazarov, A.; Mutalibkhonov, S.; Shibayama, A. Copper recovery from copper sulfide ore by combined method of collectorless flotation and additive roasting followed by acid leaching. *ChemEngineering* **2025**, *9*, 117. [CrossRef]
3. Watari, T.; Nansai, K.; Nakajima, K. Review of critical metal dynamics to 2050 for 48 elements. *Resour. Conserv. Recycl.* **2020**, *155*, 104669. [CrossRef]
4. Zhou, W.; Liu, X.; Lyu, X.; Gao, W.; Su, H.; Li, C. Extraction and separation of copper and iron from copper smelting slag: A review. *J. Clean. Prod.* **2022**, *368*, 133095. [CrossRef]
5. Godirilwe, L.L.; Gayratov, B.; Jeon, S.; Shibayama, A. Utilization of pyrite-rich tailings in sulfation roasting for efficient recovery of copper, nickel, and cobalt from smelter slag. In Proceedings of the 11th World Congress on Mechanical, Chemical, and Material Engineering (MCM25), Paris, France, 19–21 August 2025. [CrossRef]
6. Butu, A.; Rodino, S.; Butu, M. Global research progress and trends on critical metals: A bibliometric analysis. *Sustainability* **2023**, *15*, 4834. [CrossRef]
7. Lebre, E.; Corder, G.D.; Golev, A. Sustainable practices in the management of mining waste: A focus on the mineral resource. *Miner. Eng.* **2017**, *107*, 34–42. [CrossRef]
8. Gorai, B.; Jana, R. Characteristics and utilization of copper slag—A review. *Resour. Conserv. Recycl.* **2003**, *39*, 299–313. [CrossRef]
9. Zhou, C.; Ge, S.; Yu, H.; Zhang, T.; Cheng, H.; Sun, Q.; Xiao, R. Environmental risk assessment of pyrometallurgical residues derived from electroplating and pickling sludges. *J. Clean. Prod.* **2018**, *177*, 699–707. [CrossRef]
10. Khalid, M.K.; Hamuyuni, J.; Agarwal, V.; Pihlasalo, J.; Haapalainen, M.; Lundström, M. Sulfuric acid leaching for capturing value from copper rich converter slag. *J. Clean. Prod.* **2019**, *215*, 1005–1013. [CrossRef]
11. Wang, Q.; Ma, H.; Liu, M.; Guo, R.; Liu, G. A new method of full resource utilization of copper slag. *Hydrometallurgy* **2022**, *212*, 105899. [CrossRef]
12. Antonijević, M.M.; Dimitrijević, M.D.; Stevanović, Z.O.; Serbula, S.M.; Bogdanovic, G.D. Investigation of the possibility of copper recovery from the flotation tailings by acid leaching. *J. Hazard. Mater.* **2008**, *158*, 23–34. [CrossRef] [PubMed]
13. Kart, E.U.; Yazğan, Z.H.; Gümüşsoy, A. Investigation of iron selectivity behavior of copper smelter slag flotation tailing with hematitization baking and base metals leaching methods. *Physicochem. Probl. Miner. Process.* **2021**, *57*, 164–175. [CrossRef]
14. Sukla, L.B.; Panda, S.C.; Jena, P.K. Recovery of cobalt, nickel and copper from converter slag through roasting with ammonium sulphate and sulphuric acid. *Hydrometallurgy* **1986**, *16*, 153–165. [CrossRef]
15. Tümen, F.; Bailey, N.T. Recovery of metal values from copper smelter slags by roasting with pyrite. *Hydrometallurgy* **1990**, *25*, 317–328. [CrossRef]
16. Altundogan, H.S.; Tümen, F. Metal recovery from copper converter slag by roasting with ferric sulphate. *Hydrometallurgy* **1997**, *44*, 261–267. [CrossRef]
17. Zhang, Y.; Man, R.; Ni, W.; Wang, H. Selective leaching of base metals from copper smelter slag. *Hydrometallurgy* **2010**, *103*, 25–29. [CrossRef]
18. Perederiy, I.; Papangelakis, V.G.; Buarzaiga, M.; Mihaylov, I. Co-treatment of converter slag and pyrrhotite tailings via high-pressure oxidative leaching. *J. Hazard. Mater.* **2011**, *194*, 399–406. [CrossRef] [PubMed]
19. Kaksonen, A.H.; Sarkijarvi, S.; Puhakka, J.A.; Peuraniemi, E.; Junnikkala, S.; Tuovinen, O.H. Solid phase changes in chemically and biologically leached copper smelter slag. *Miner. Eng.* **2017**, *106*, 97–101. [CrossRef]

20. Zhang, C.; Hu, B.; Wang, H.; Wang, M.; Wang, X. Recovery of valuable metals from copper slag. *Min. Metall. Explor.* **2020**, *37*, 1241–1251. [CrossRef]
21. Zhang, S.; Zhu, N.; Mao, F.; Zhang, J.; Huang, X.; Li, F.; Li, X.; Wu, P.; Dang, Z. A novel strategy for harmlessness and reduction of copper smelting slags by alkali disaggregation of fayalite (Fe_2SiO_4) coupling with acid leaching. *J. Hazard. Mater.* **2021**, *402*, 123791. [CrossRef] [PubMed]
22. Wan, X.; Taskinen, P.; Shi, J.; Jokilaakso, A. A potential industrial waste–waste co-treatment process of utilizing waste SO_2 gas and residue heat to recover Co, Ni, and Cu from copper smelting slag. *J. Hazard. Mater.* **2021**, *414*, 125541. [CrossRef] [PubMed]
23. Godirilwe, L.L.; Haga, K.; Altansukh, B.; Jeon, S.; Danha, G.; Shibayama, A. Establishment of a hydrometallurgical scheme for the recovery of copper, nickel, and cobalt from smelter slag and its economic evaluation. *Sustainability* **2023**, *15*, 10496. [CrossRef]
24. Phiri, T.C.; Singh, P.; Hara, Y.S.; Siame, J.; Nikoloski, A.N. Carbothermic reduction of copper slag in the presence of borax. *Miner. Process. Extr. Metall. Rev.* **2023**, *46*, 165–176. [CrossRef]
25. Piatak, N.M.; Parsons, M.B.; Seal, R.R. Characteristics and environmental aspects of slag: A review. *Appl. Geochem.* **2015**, *57*, 236–266. [CrossRef]
26. Zhou, H.; Liu, G.; Zhang, L.; Zhou, C. Mineralogical and morphological factors affecting the separation of copper and arsenic in flash copper smelting slag flotation beneficiation process. *J. Hazard. Mater.* **2021**, *401*, 123293. [CrossRef] [PubMed]
27. Bulut, G.; Perek, K.T.; Gül, A.; Arslan, F.; Önal, G. Recovery of metal values from copper slags by flotation and roasting with pyrite. *Min. Metall. Explor.* **2007**, *24*, 13–18. [CrossRef]
28. Li, Y.; Papangelakis, V.G.; Perederiy, I. High-pressure oxidative acid leaching of nickel smelter slag: Characterization of feed and residue. *Hydrometallurgy* **2009**, *97*, 185–193. [CrossRef]
29. Zhang, H.; Hu, C.; Gao, W.; Lu, M. Recovery of iron from copper slag using coal-based direct reduction: Reduction characteristics and kinetics. *Minerals* **2020**, *10*, 973. [CrossRef]
30. Phiri, T.C.; Singh, P.; Nikoloski, A.N. The potential for copper slag waste as a resource for a circular economy: A review—Part II. *Miner. Eng.* **2021**, *172*, 107150. [CrossRef]
31. Perederiy, I.; Papangelakis, V.G. Why amorphous FeO–SiO_2 slags do not acid-leach at high temperatures. *J. Hazard. Mater.* **2017**, *321*, 737–744. [CrossRef] [PubMed]
32. Liao, Y.; Ji, G.; Shi, G.; Xi, J. A study on the selective leaching of valuable metals and the configuration of iron silicon phases in copper smelting slag by oxidative pressure leaching. *J. Sustain. Metall.* **2021**, *7*, 1143–1153. [CrossRef]
33. Shibayama, K.; Yokogawa, T.; Sato, H.; Enomoto, M.; Nakai, O.; Ito, T.; Mizuno, F.; Hattori, Y. Taganito HPAL plant project. *Miner. Eng.* **2016**, *88*, 61–65. [CrossRef]
34. Tian, Q.H.; Dong, B.; Guo, X.Y.; Wang, Q.A.; Xu, Z.P.; Li, D. Valuable metals substance flow analysis in high-pressure acid leaching process of laterites. *J. Cent. South Univ.* **2023**, *30*, 1776–1786. [CrossRef]
35. Min, X.; Jiang, G.; Wang, Y.; Zhou, B.; Xue, K.; Ke, Y.; Xu, Q.; Wang, J.; Ren, H. Sulfidation roasting of zinc leaching residue with pyrite for recovery of zinc and iron. *J. Cent. South Univ.* **2020**, *27*, 1186–1196. [CrossRef]
36. Wen, X.; Feng, D.; Li, M.; Zhang, X.; Zhang, H.; Kang, J.; Zhang, H. Sulfidation behavior and mechanism of hemimorphite via microwave roasting with pyrite. *Can. Metall. Q.* **2025**, 1–14. [CrossRef]
37. Zhang, Y.; Li, Q.; Liu, X.; Xu, B.; Yang, Y.; Jiang, T. A thermodynamic analysis on the roasting of pyrite. *Minerals* **2019**, *9*, 220. [CrossRef]
38. Hietala, M. *HSC Chemistry for Windows*, Version 10.7.2.0; Outotec Research: Pori, Finland, 2025.
39. Kar, B.B.; Swamy, Y.V.; Murthy, B.V.R. Design of experiments to study the extraction of nickel from lateritic ore by sulphatization using sulphuric acid. *Hydrometallurgy* **2000**, *56*, 387–394. [CrossRef]
40. Liu, Y.; Lv, X.; You, Z.; Lv, X. Kinetics study on non-isothermal carbothermic reduction of nickel laterite ore in presence of Na_2SO_4. *Powder Technol.* **2020**, *362*, 486–492. [CrossRef]
41. Sun, Q.; Cheng, H.; Mei, X.; Liu, Y.; Li, G.; Xu, Q.; Lu, X. Efficient synchronous extraction of nickel, copper, and cobalt from low–nickel matte by sulfation roasting–water leaching process. *Sci. Rep.* **2020**, *10*, 9916. [CrossRef] [PubMed]
42. Liu, X.W.; Feng, Y.L.; Li, H.R.; Yang, Z.C.; Cai, Z.L. Recovery of valuable metals from a low-grade nickel ore using an ammonium sulfate roasting–leaching process. *Int. J. Miner. Metall. Mater.* **2012**, *19*, 377–383. [CrossRef]
43. Siriwardane, R.V.; Poston, J.A.; Fisher, E.P.; Shen, M.S.; Miltz, A.L. Decomposition of the sulfates of copper, iron (II), iron (III), nickel, and zinc: XPS, SEM, DRIFTS, XRD, and TGA study. *Appl. Surf. Sci.* **1999**, *152*, 219–236. [CrossRef]
44. Dimitrijevic, M.D.; Urosevic, D.M.; Jankovic, Z.D.; Milic, S.M. Recovery of copper from smelting slag by sulphation roasting and water leaching. *Physicochem. Probl. Miner. Process.* **2016**, *52*, 409–421. [CrossRef]
45. Yu, D.; Utigard, T.A.; Barati, M. Fluidized bed selective oxidation–sulfation roasting of nickel sulfide concentrate: Part II. Sulfation roasting. *Metall. Mater. Trans. B* **2014**, *45*, 653–661. [CrossRef]
46. Li, G.; Cheng, H.; Chen, S.; Lu, X.; Xu, Q.; Lu, C. Mechanism of Na_2SO_4 promoting nickel extraction from sulfide concentrates by sulfation roasting–water leaching. *Metall. Mater. Trans. B* **2018**, *49*, 1136–1148. [CrossRef]

47. Ntakamutshi, P.T.; Kime, M.B.; Mwema, M.E.; Ngenda, B.R.; Kaniki, T.A. Agitation and column leaching studies of oxidised copper-cobalt ores under reducing conditions. *Miner. Eng.* **2017**, *111*, 47–54. [CrossRef]
48. Tshipeng, S.Y.; Kaniki, A.T.; Kime, M.B. Effects of the addition points of reducing agents on the extraction of copper and cobalt from oxidized copper-cobalt ores. *J. Sustain. Metall.* **2017**, *3*, 823–828. [CrossRef]
49. Hu, J.H.; Wang, H.; Zhao, L.M.; Li, L.; Liu, H.L. Characterization of copper slag from impoverishment. *J. Saf. Environ.* **2011**, *11*, 90–93. [CrossRef]
50. Peak, D.; Ford, R.G.; Sparks, D. An in situ ATR-FTIR investigation of sulfate bonding mechanisms on goethite. *J. Colloid Interface Sci.* **1999**, *218*, 289–299. [CrossRef] [PubMed]
51. Salama, W.; El Aref, M.; Gaupp, R. Spectroscopic characterization of iron ores formed in different geological environments using FTIR, XPS, Mössbauer spectroscopy and thermoanalyses. *Spectrochim. Acta Part A Mol. Biomol. Spectrosc.* **2015**, *136*, 1816–1826. [CrossRef] [PubMed]
52. Botelho Junior, A.B.; Dreisinger, D.B.; Espinosa, D.C.R. A review of nickel, copper, and cobalt recovery by chelating ion exchange resins from mining processes and mining tailings. *Min. Metall. Explor.* **2019**, *36*, 199–213. [CrossRef]
53. Mohammed, T.; Bezuidenhout, G.A.; Oraby, E.A.; Eksteen, J.J. Sequential separation of cobalt, copper, and nickel from alkaline glycinate solutions using solvent extraction. *J. Sustain. Metall.* **2024**, *10*, 2455–2468. [CrossRef]
54. Sole, K.C. Solvent extraction in the hydrometallurgical processing and purification of metals: Process design and selected applications. In *Solvent Extraction and Liquid Membranes: Fundamentals and Applications in New Materials*; CRC Press: Boca Raton, FL, USA, 2008; pp. 141–200.
55. Mackay, I.; Mendez, E.; Molina, I.; Videla, A.R.; Cilliers, J.J.; Brito-Parada, P.R. Dynamic froth stability of copper flotation tailings. *Miner. Eng.* **2018**, *124*, 103–107. [CrossRef]
56. Moncur, M.C.; Jambor, J.L.; Ptacek, C.J.; Blowes, D.W. Mine drainage from the weathering of sulfide minerals and magnetite. *Appl. Geochem.* **2009**, *24*, 2362–2373. [CrossRef]
57. Baghalha, M.; Papangelakis, V.G.; Curlook, W. Factors affecting the leachability of Ni/Co/Cu slags at high temperature. *Hydrometallurgy* **2007**, *85*, 42–52. [CrossRef]
58. Mu, W.; Cheng, H.; Xu, J.; Luo, S.; Zhai, Y.; Xu, Q. Extraction of valuable metals from low-grade nickel matte by $FeCl_3 \cdot 6H_2O$ roasting and water leaching process with studies on phase evolution and kinetics analysis of chlorination process. *Hydrometallurgy* **2021**, *202*, 105614. [CrossRef]

Disclaimer/Publisher's Note: The statements, opinions and data contained in all publications are solely those of the individual author(s) and contributor(s) and not of MDPI and/or the editor(s). MDPI and/or the editor(s) disclaim responsibility for any injury to people or property resulting from any ideas, methods, instructions or products referred to in the content.